

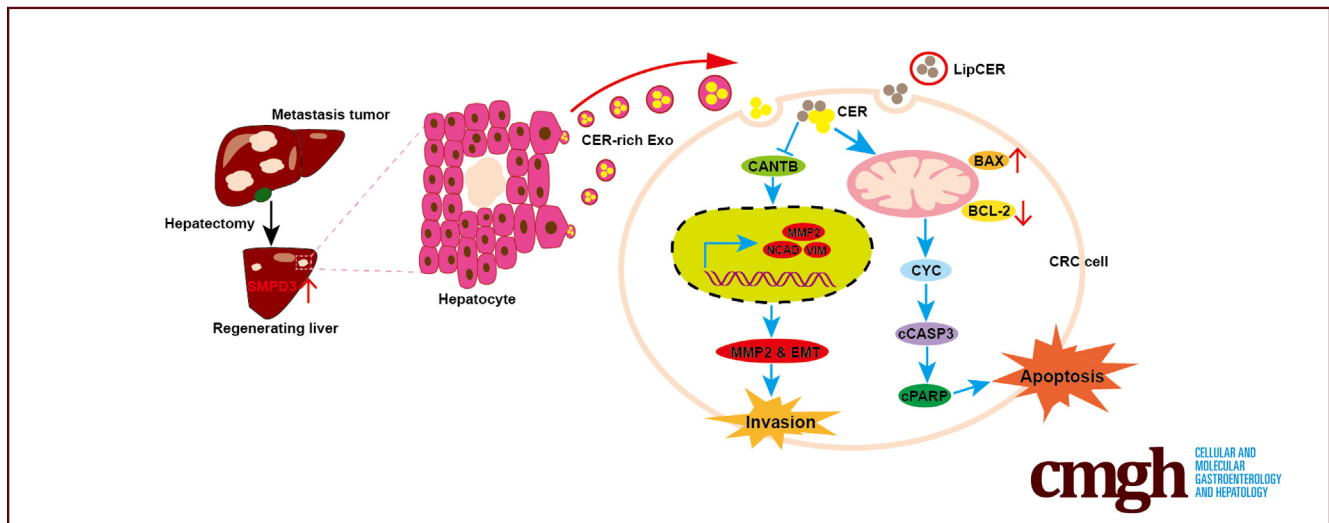
ORIGINAL RESEARCH

Activation of Sphingomyelin Phosphodiesterase 3 in Liver Regeneration Impedes the Progression of Colorectal Cancer Liver Metastasis Via Exosome-Bound Intercellular Transfer of Ceramides



Qingping Li,^{1,*} Jiyeuan Li,^{2,*} Kai Wang,^{2,*} Leyi Liao,² Yiyi Li,³ Hanbiao Liang,² Can Huang,² Jian Gan,² Xiaoyu Dong,¹ Yaowen Hu,¹ Jiaxin Cheng,¹ Hongli Ji,¹ Cuiting Liu,⁴ Minghui Zeng,⁵ Sheng Yu,² Biao Wang,² Jianping Qian,² Zhongshun Tang,⁶ Yonghong Peng,⁴ Shanhua Tang,² Mengxuan Li,⁶ Jie Zhou,² Jun Yan,¹ and Chuanjiang Li²

¹Department of General Surgery, Guangdong Provincial Key Laboratory of Precision Medicine for Gastrointestinal Tumor, Nanfang Hospital, The First School of Clinical Medicine, Southern Medical University, Guangzhou, Guangdong, China; ²Division of Hepatobiliarypancreatic Surgery, Department of General Surgery, Nanfang Hospital, The First School of Clinical Medicine, Southern Medical University, Guangzhou, Guangdong, China; ³Department of Radiation Oncology, Nanfang Hospital, The First School of Clinical Medicine, Southern Medical University, Guangzhou, Guangdong, China; ⁴Central Laboratory, Southern Medical University, Guangzhou, Guangdong, China; ⁵Institute of Scientific Research, Southern Medical University, Guangzhou, Guangdong, China; and ⁶The First Clinical College, Southern Medical University, Guangzhou, Guangdong, China



SUMMARY

Induction of liver regeneration (LR) resulted in significant up-regulation of hepatic sphingomyelin phosphodiesterase 3 (SMPD3). SMPD3-produced exosomal ceramide (CER) constitutes a critical anti-colorectal cancer liver metastasis (CRLM) mechanism in LR to impede the progression of CRLM.

BACKGROUND & AIMS: The machinery that prevents colorectal cancer liver metastasis (CRLM) in the context of liver regeneration (LR) remains elusive. Ceramide (CER) is a potent anti-cancer lipid involved in intercellular interaction. Here, we investigated the role of CER metabolism in mediating the interaction between hepatocytes and metastatic colorectal cancer (CRC) cells to regulate CRLM in the context of LR.

METHODS: Mice were intrasplenically injected with CRC cells. LR was induced by 2/3 partial hepatectomy (PH) to mimic the CRLM in the context of LR. The alteration of corresponding CER-metabolizing genes was examined. The biological roles of CER metabolism in vitro and in vivo were examined by performing a series of functional experiments.

RESULTS: Induction of LR augmented apoptosis but promoted matrix metalloproteinase 2 (MMP2) expression and epithelial-mesenchymal transition (EMT) to increase the invasiveness of metastatic CRC cells, resulting in aggressive CRLM. Up-regulation of sphingomyelin phosphodiesterase 3 (SMPD3) was determined in the regenerating hepatocytes after LR induction and persisted in the CRLM-adjacent hepatocytes after CRLM formation. Hepatic Smpd3 knockdown was found to further promote CRLM in the context of LR by abolishing mitochondrial apoptosis and augmenting the invasiveness in metastatic CRC cells by up-regulating MMP2 and EMT through promoting the nuclear translocation of β -catenin.

Mechanistically, we found that hepatic SMPD3 controlled the generation of exosomal CER in the regenerating hepatocytes and the CRLM-adjacent hepatocytes. The SMPD3-produced exosomal CER critically conducted the intercellular transfer of CER from the hepatocytes to metastatic CRC cells and impeded CRLM by inducing mitochondrial apoptosis and restricting the invasiveness in metastatic CRC cells. The administration of nanoliposomal CER was found to suppress CRLM in the context of LR substantially.

CONCLUSIONS: SMPD3-produced exosomal CER constitutes a critical anti-CRLM mechanism in LR to impede CRLM, offering the promise of using CER as a therapeutic agent to prevent the recurrence of CRLM after PH. (*Cell Mol Gastroenterol Hepatol* 2023;16:385–410; <https://doi.org/10.1016/j.jcmgh.2023.05.007>)

Keywords: Liver Regeneration; CRLM; SMPD3; CER.

The liver represents the most frequent site for colorectal cancer (CRC) metastases.¹ More than 50% of CRC patients develop CRC liver metastasis (CRLM) during their lifetime.² Partial hepatectomy (PH) is still the primary treatment of CRLM.³ However, approximately 40% of CRLM patients develop intrahepatic recurrence, with the majority recurring within only 6 months after PH.⁴ PH is known to induce liver regeneration (LR) that critically alters the property of cancer surveillance against CRLM in the hepatic microenvironments.^{5,6} However, the role of LR in regulating the malignancy of CRLM has not yet been fully elucidated. Animal studies demonstrated that LR induced by PH promotes the growth of CRLM.^{7–9} Oppositely, LR was found to impede the progression of CRLM by reducing the growth of CRLM without increasing the recurrence of CRLM.^{10–12} Because LR is a comprehensive process tightly regulated by various signaling molecules involved in the progression of CRLM, the regenerating liver may contain both anti-cancer and pro-cancer molecular constituents that interact with metastatic CRC cells, exerting distinct regulatory effects on CRLM.^{5,6,13} There is an unmet need to investigate the anti-cancer machinery that safeguards against CRLM in the regenerating liver after PH.


Ceramide (CER) is a class of bioactive sphingolipids with potent anti-cancer activities involved in intercellular interaction.^{14–16} CER is generated via the de novo, catabolic, and salvage pathway, and it is degraded by ceramidases to produce sphingosine (SPH) and sphingosine-1-phosphate (S1P).¹⁷ CER is known to inhibit the progression of various cancer by inducing cell-cycle arrest, apoptosis, and senescence, as well as reducing the invasiveness of migration and invasion in cancer including CRC.^{18–20} Studies have demonstrated that nanoliposomal CER (LipCER) is an efficacious anti-cancer agent with potential clinical applications in cancer treatment.^{21–23} Notably, CER is enriched in exosomes that are essential components of intercellular interaction in the cancer microenvironment,^{24–26} and CER generation catalyzed by sphingomyelin phosphodiesterase 3 (SMPD3) critically controls the formation and release of exosomes.²⁴ Activation of SMPD3-catalyzed CER generation was found in the remanent liver after PH and was correlated

with the proliferation of hepatocytes during LR after PH.^{27,28} However, the function of exosomal CER in modulating the intercellular communication between hepatocytes and metastatic CRC cells has not been elucidated. Recently, Zietzer et al²⁹ reported that intercellular transfer of CER via extracellular vesicles induced apoptosis in endothelial cells, indicating that CER in extracellular vesicles is still capable of inducing cell death in target cells. Therefore, it is worth testing whether exosomal CER acts as an extracellular anti-cancer signalosome to prevent CRLM in the regenerating liver.

In this study, we investigated the role of CER metabolism in regulating CRLM in the context of PH-induced LR. Our data demonstrated that the SMPD3-produced exosomal CER in hepatocytes impedes CRLM by inducing mitochondrial apoptosis and restricting the invasiveness of metastatic CRC cells in the context of LR. Importantly, treatment of LipCER remarkably suppresses CRLM in the context of LR by inducing apoptosis and reducing the invasiveness of metastatic CRC cells. These findings highlight that SMPD3-produced exosomal CER constitutes a critical anti-CRLM mechanism that impedes the progression of CRLM in the context of PH-induced LR. These discoveries also present the potential for using CER as a therapeutic approach to prevent CRLM recurrence after PH.

*Authors share co-first authorship.

Abbreviations used in this paper: AAV, adeno-associated virus; ACER2, alkaline ceramidase 2; ACER3, alkaline ceramidase 3; ACTB, β -actin; B4GALT6, beta-1,4-galactosyltransferase 6; CANTB, β -catenin; cCASP, cleaved caspase; cPARP, cleaved poly ADP-ribose polymerase; CER, ceramides; CERG2, diglycosylceramide; CERK, ceramide kinase; CERKL, ceramide kinase like; CERS, ceramide synthase; CERT, ceramide transfer protein; CRC, colorectal cancer; CRLM, colorectal cancer liver metastasis; DEGS1, delta(4)-desaturase 1; DEGS2, delta(4)-desaturase 2; ECAD, E-cadherin; EMT, epithelial mesenchymal changes; ENPP7, alkaline sphingomyelinase 3; GALC, galactosylceramidase; GBA1, glucosylceramidase beta 1; GBA2, glucosylceramidase beta 2; GLA, galactosidase; GSL, glycerophospholipids; LipCER, nanoliposomal CER; LR, liver regeneration; MMP, matrix metalloproteinase; NAAA, N-acylthanolamine acid amidase; NCAD, N-cadherin; NTA, nanoparticle tracking analysis; PCNA, proliferating cell nuclear antigen; PCR, polymerase chain reaction; PH, partial hepatectomy; PH-CRLM, colorectal cancer liver metastasis after partial hepatectomy; SAMD8, sphingomyelin synthase-related protein 1; SGMS1, sphingomyelin synthase 1; SGMS2, sphingomyelin synthase 2; SGPL1, sphingosine-1-phosphate lyase; SGPP1, sphingosine-1-phosphate phosphatase 1; SGPP2, sphingosine-1-phosphate phosphatase 2; SM, sphingomyelins; SMases, sphingomyelinases; SMPD1, acid sphingomyelinase; SMPD2, neutral sphingomyelinase 1; SMPD3, sphingomyelin phosphodiesterase 3; SMPD4, neutral sphingomyelinase 3; SMPD5, mitochondrial-associated neutral sphingomyelinase; SMPDL3A, acid sphingomyelinase like 3A; SMPDL3B, acid sphingomyelinase like 3B; SPF, specific pathogen-free; SPH, sphingosines; SPHK1, sphingosine kinase 1; SPHK2, sphingosine kinase 2; SPTLC1, serine palmitoyltransferase 1; S1P, sphingosine 1 phosphate; S1PR1, S1P receptor 1; S1PR2, S1P receptor 2; S1PR3, S1P receptor 3; S1PR4, S1P receptor 4; S1PR5, S1P receptor 5; TUNEL, terminal deoxynucleotidyl transferase dUTP nick end labeling; UGCG, UDP-glucose ceramide glucosyltransferase; VIM, vimentin.

 Most current article

© 2023 The Authors. Published by Elsevier Inc. on behalf of the AGA Institute. This is an open access article under the CC BY-NC-ND license (<http://creativecommons.org/licenses/by-nc-nd/4.0/>).

2352-345X

<https://doi.org/10.1016/j.jcmgh.2023.05.007>

Results

Induction of LR Regulates CRLM Bidirectionally by Augmenting Apoptosis and Enhancing Invasiveness in Metastatic CRC Cells

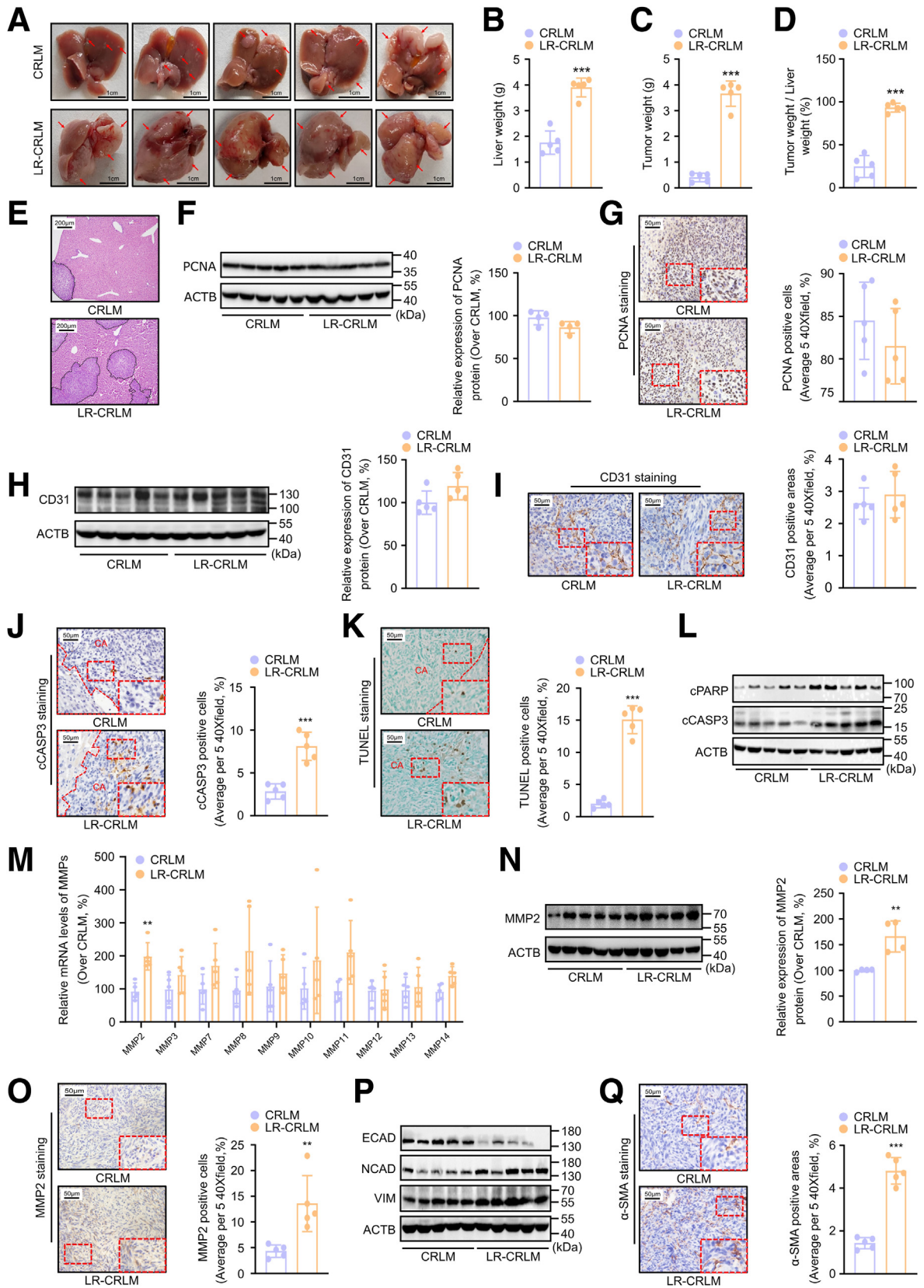
To investigate the impact of LR on CRLM, we implanted mouse CRC cells in the spleen and induced LR by 2/3 PH. Thus, the CRC cells would colonize in the regenerating liver from the spleen through the portal vein, which mimicked the most common metastatic path of CRLM.^{7,9} We found that the weight and territory of macroscopic CRLM were increased in the remnant liver after PH compared with the CRLM in the normal liver, suggesting that induction of LR by PH promotes the colonization and territorial expansion of CRLM (Figure 1A–E). Notably, although CRLM grew locally in the normal liver, it diffusely spread in the remnant liver after PH (Figure 1A). Next, we investigated the effects of LR on the proliferation, angiogenesis, apoptosis, and invasiveness of CRLM. Determination of proliferation and angiogenesis markers demonstrated that the induction of LR did not significantly affect the proliferation and angiogenesis in metastatic CRC cells (Figure 1F–J). However, examination of apoptosis by cleaved caspase 3 (cCASP3), cleaved poly ADP-ribose polymerase (cPARP), and terminal deoxynucleotidyl transferase dUTP nick end labeling (TUNEL) staining demonstrated that the number of apoptotic CRC cells and the protein levels of cCASP3 and cPARP were remarkably increased in CRLM in the remnant liver after PH compared with those in the normal liver (Figure 1J–L), suggesting that induction of LR substantially enhances apoptosis in metastatic CRC cells. Matrix metalloproteinases (MMPs) and epithelial-mesenchymal transition (EMT) constitute cancer invasiveness.^{30–32} Because the induction of LR exaggerated the territorial expansion of CRLM, we tested whether induction of LR altered the expression of MMPs and EMT in metastatic CRC cells. We found that MMP2 was robustly up-regulated in CRC cells in the remnant liver after PH compared with those in the normal liver, suggesting induction of LR promotes MMP2 up-regulation in CRLM (Figure 1M–O). Immunoblotting of EMT markers revealed a reduction in epithelial markers (E-cadherin [ECAD]) and an increase in mesenchymal markers (N-cadherin [NCAD] and vimentin [VIM]) in CRC cells of CRLM in the remnant liver after PH, suggesting that induction of LR promotes EMT in CRLM (Figure 1P). In addition, immunostaining of α -SMA, another marker of EMT,³³ demonstrated that the number of α -SMA positive cells was significantly increased in CRLM in the remnant liver after PH compared with those in the normal liver (Figure 1Q), suggesting that induction of LR facilitates EMT of metastatic CRC cells. These data demonstrate that induction of LR bidirectionally regulates CRLM by augmenting apoptosis and enhancing invasiveness in metastatic CRC cells, resulting in the aggressive progression of CRLM.

Up-regulation of SMPD3 in LR Impedes CRLM by Inducing Mitochondrial Apoptosis and Restricting the Invasiveness of Metastatic CRC Cells

Dysregulation of CER metabolism has been found in the regenerating liver^{27,28,34} and is known to regulate apoptosis

and invasiveness in cancer critically.^{20,35} Recently, CER and the relevant enzymes have been found to mediate the interaction between cancer cells and parenchyma cells through exosomes or paracrine fashion.^{25,26} To investigate whether CER metabolism was involved in regulating CRLM in the regenerating liver, we first screened the dysregulation of CER metabolic enzymes in CRLM and CRLM-adjacent liver tissues. Quantitative polymerase chain reaction (PCR) arrays of CER metabolic enzymes demonstrated that induction of LR resulted in significant up-regulation of *Smpd3*, sphingosine-1-phosphate phosphatase 2 (*Sgpp2*), delta(4)-desaturase 1 (*Degs1*), delta(4)-desaturase 2 (*Degs2*), beta-1,4-galactosyltransferase 6 (*B4galt6*), and acid sphingomyelinase like 3B (*Smpdl3b*) in CRLM-adjacent liver tissues (Figure 2A). However, the mRNA levels of CER metabolic enzymes did not significantly differ between CRLM in the normal liver and CRLM in the remnant liver after PH (Figure 2B). These data suggest that the induction of LR causes dysregulation of CER metabolism in CRLM-adjacent liver tissues without affecting the intrinsic CER metabolism in CRLM.

SMPD3 is known to regulate cancer malignancy by producing CER^{36–38} and is involved in LR.^{27,28} Because *Smpd3* was found to be the most robustly up-regulated enzyme in response to LR in CRLM-adjacent liver tissues (Figure 2A), we proceeded to investigate the role of SMPD3 in regulating CRLM in the context of LR. We first performed immunoblotting and immunostaining of SMPD3 and confirmed that the induction of LR up-regulated the protein levels of SMPD3 in CRLM-adjacent hepatocytes (Figure 2C–E). In addition, by measuring the expression of SMPD3 in the regenerating liver tissues without intrasplenic implantation of CRC cells at both early (postoperative day 3) and late stages (postoperative day 14) after PH, we found that the SMPD3 was intrinsically up-regulated in hepatocytes of the regenerating liver at the early stage after PH but receded at the late stage (Figure 3A–C), suggesting that the presence of CRLM might be necessary for sustaining the LR-induced up-regulation of SMPD3 in the CRLM-adjacent hepatocytes. To further investigate the pathologic functions of SMPD3 in CRLM in the context of LR, mouse hepatic SMPD3 was knocked down by injection of liver-directed adeno-associated virus (AAV) carrying an sh*Smpd3* vector along with a GFP reporter gene (Figure 3D and E). We first found that *Smpd3* knockdown did not significantly impact the process of LR in mice, including body weight, liver weight, and hepatocellular proliferation (Figure 3F–J). Then, the CRLM model was established in the *Smpd3* knockdown and the control mice with or without 2/3 PH (Figure 4A). We found that *Smpd3* knockdown promoted CRLM in the normal liver and further exaggerated the progression of CRLM in the remnant liver after PH, indicated by increases in weight and territory of macroscopic CRLM (Figure 4B–F). Examinations of apoptosis by cCASP3 and TUNEL staining demonstrated that *Smpd3* knockdown alleviated apoptosis in CRLM more profoundly in the remnant liver after PH than in the normal liver (Figure 4G and H). Mechanistically, we found that *Smpd3* knockdown nearly abolished the activation of the mitochondrial pathway of apoptosis in CRLM in the remnant liver after PH, indicated by the increase of BCL-2 and the



reduction of BAX, CYC, cPARP, and cCASP3 in CRLM of hepatic Smpd3 knockdown mice (Figure 4I). These data highlight the anti-CRLM role of SMPD3 in hepatocytes by inducing apoptosis in metastatic CRC cells in the context of LR. Next, examination of MMP2 and EMT markers demonstrated that Smpd3 knockdown significantly augmented the up-regulation of MMP2 and further facilitated EMT of CRLM in the remnant liver after PH and the normal liver (Figure 4J–L). Notably, the positive effects of Smpd3 knockdown on MMP2 up-regulation and EMT were more profound in CRLM in the remnant liver after PH than in the normal liver, suggesting SMPD3 restricts the increase in the invasiveness of CRLM, particularly in the context of LR (Figure 4J–L). Studies have shown that dysregulation of the Wnt/ β -catenin (CANTB) signaling pathway leads to EMT, which is characterized by the nuclear translocation of CANTB.^{39–42} The accumulation of nuclear CANTB can also activate MMP2 expression.^{43–45} To determine the potential mechanisms underlying the role of SMPD3 in regulating the MMP2 and EMT of CRLM in the context of LR, we investigated the nuclear translocation of CANTB. Induction of LR was found to significantly increase the CANTB expression in the nuclear fractions in metastatic CRC cells of CRLM (Figure 4M and N). Notably, knockdown of Smpd3 further increased the nuclear expression of CANTB in metastatic CRC cells of CRLM in the remnant liver after PH and the normal liver (Figure 4M and N), suggesting that SMPD3 limited the up-regulation of MMP2 and EMT likely by suppressing the nuclear translocation of CANTB in CRC cells of CRLM. These data suggest that the up-regulation of hepatic SMPD3 in LR impedes the progression of CRLM by inducing apoptosis and prohibiting the invasiveness of metastatic CRC cells.

Hepatic SMPD3 Preserves the Anti-CRLM Properties of LR-Derived Exosomes by Maintaining Their Pro-apoptotic and Anti-invasive Activities

Exosomes are essential for parenchyma cells to interact with metastatic cancer cells.^{42,46} SMPD3 is known to control the release of exosomes by producing CER,^{24,25,29} but the

anti-cancer role of SMPD3-produced exosomal CER has not yet been elucidated. We investigated whether exosomes conducted the regulatory effects of LR induction on CRLM and how SMPD3 regulated the effects of LR-derived exosomes on CRLM. We isolated the LR-derived serum exosomes (LR-Exo) from mice at postoperative day 3 after PH, when the mouse liver was regenerating with hepatocellular proliferation (Figure 5A). Exosomes isolated from the mice that received sham surgery were used as the vehicle control (Sham-Exo). Purified exosomes were examined by transmission electron microscopy, revealing the typical size (50–150 nm) and a bilayer cup-shaped morphology of exosomes (Figure 5B). NTA revealed that the isolated exosomes had a similar size distribution of 100–150 nm in diameter, with a peak at approximately 100 nm (Figure 5C). Immunoblotting confirmed the presence of exosome biomarkers in the isolated exosomes, including HSP90, HSP70, CD9, and CD63 (Figure 5D). Then, we investigated the regulatory effects of exosomes on MC38 cells. In vitro uptake of exosomes by MC38 cells was confirmed by labeling the exosomes with PKH67, and there was no significant difference in the uptake between LR-Exo and Sham-Exo by the MC38 cells (Figure 5E). Notably, we found that LR-Exo treatment significantly increased the migratory and invasive capacity of MC38 cells (Figure 5F), suggesting that exosomes were capable of mediating the regulatory effects of LR on CRC cells.

To investigate whether SMPD3 preserved the anti-cancer effects of LR-derived exosomes on MC38 cells, we isolated the LR-derived serum exosomes from Smpd3 knockdown (shSmpd3-LR-Exo) and their control mice (shCON-LR-Exo) at postoperative day 3 after PH or sham surgery (shSmpd3-sham-Exo, shCON-sham-Exo) (Figure 5G). In vitro study demonstrated that Smpd3 knockdown substantially potentiated the pro-invasive effects of LR-derived exosomes on MC38 cells, while reducing the pro-apoptotic effects of LR-derived exosomes (Figure 5H–J). Next, we investigated the regulatory effects of exosome injection on CRLM in the normal liver in vivo. The assessment of exosome uptake confirmed that there

Figure 1. (See previous page). Induction of LR regulates CRLM bidirectionally by augmenting apoptosis and enhancing invasiveness in metastatic CRC cells. C57BL/6J mice were injected intrasplenically with MC38 cells, followed by splenectomy. Then mice of the LR-CRLM group were subjected to 2/3 hepatectomy to induce LR after injection of MC38 cells. Mice of the control group (CRLM) were subjected to intrasplenic injection of MC38 cells without hepatectomy. Fourteen days after surgery, mice were killed, and tissues were collected for examination. (A–E) Pathology of the CRLM in mice with and without LR induction. (A) Morphology of CRLM; arrows indicate CRLM. (B) Mouse liver weight. (C) Mouse macroscopic tumor weight. (D) Ratio of macroscopic tumor weight and liver weight in mice. (E) H&E staining of liver sections; dotted line area indicates the area of CRLM. (F and G) Examination on proliferation in CRLM of mice with and without LR induction. (F) Immunoblotting of PCNA and quantification of protein levels of PCNA in CRLM. (G) Immunostaining of PCNA and quantification of PCNA-positive cells in CRLM. (H and I) Examination on angiogenesis in CRLM of mice with and without LR induction. (H) Immunoblotting of CD31 and quantification of protein levels of CD31 in CRLM. (I) Immunostaining of CD31 and quantification of CD31-positive areas in CRLM. (J–L) Examination on apoptosis in CRLM of mice with and without LR induction. (J) Immunostaining of cCASP3 and quantification of cCASP3-positive cells in CRLM. (K) TUNEL staining and quantification of TUNEL-positive cells in CRLM. (L) Immunoblotting of cCASP3 and cPARP on proteins extracted from CRLM tissues. (M–O) Measurement of MMPs expression in CRLM of mice with and without LR induction. (M) Quantitative PCR arrays of mRNA levels of MMPs in CRLM. (N) Immunoblotting of MMP2 and quantification of protein levels of MMP2 in CRLM. (O) Immunostaining of MMP2 and quantification of MMP2-positive cells in CRLM. (P and Q) Evaluation of EMT in CRLM of mice with and without LR induction. (P) Immunoblotting of EMT markers, including NCAD, ECAD, and VIM. (Q) Immunostaining of α -SMA and quantification of α -SMA-positive areas in CRLM. Images in E, G, I, J, K, O, and Q represent results from 1 of 5 pairs of mice in each group. Data in B, C, D, F, G, H, I, J, K, M, N, O, and Q were expressed as mean \pm standard deviation, n = 5 in each group. **P < 0.01, ***P < 0.001.

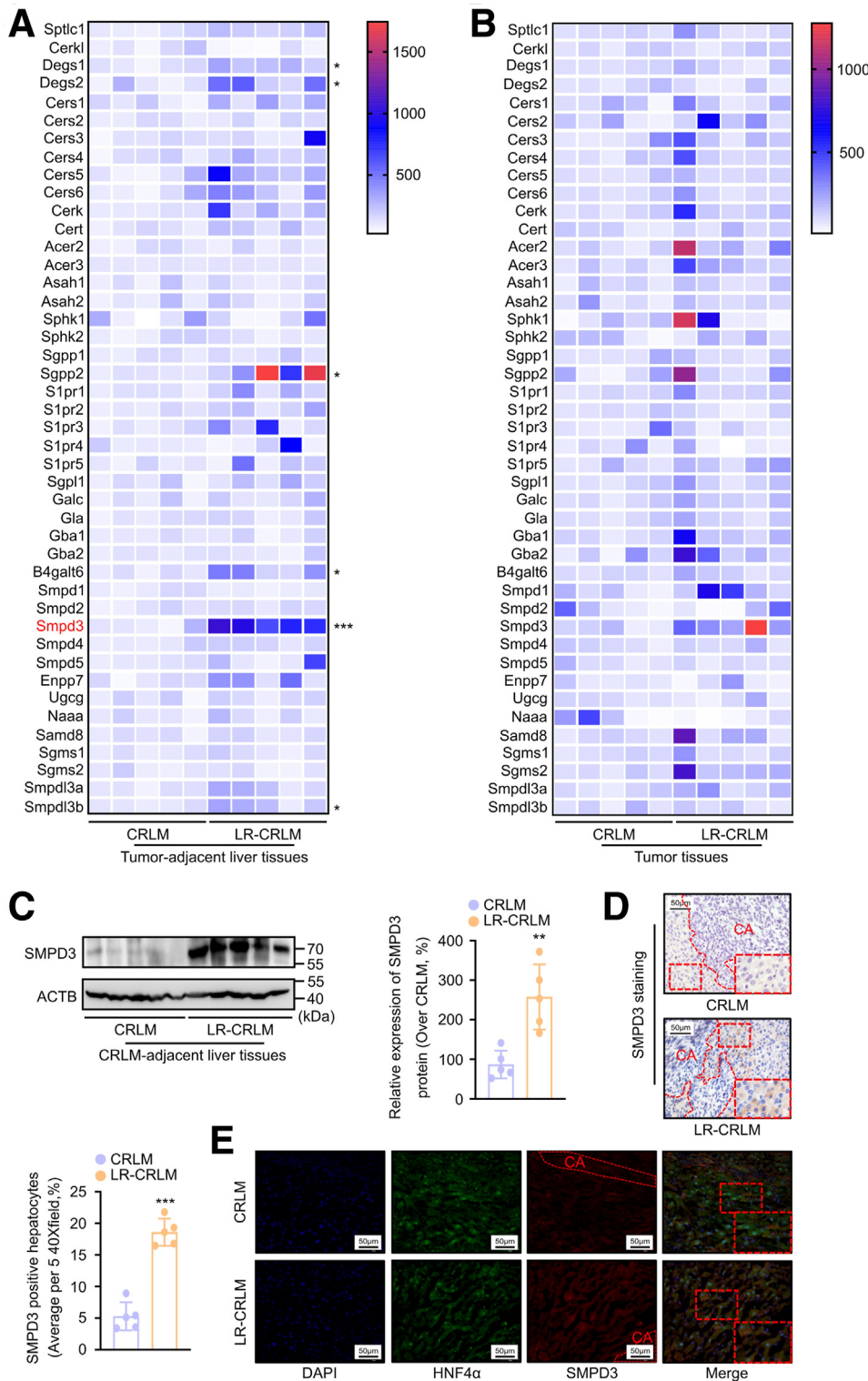


Figure 2. Up-regulation of SMPD3 in CRLM-adjacent liver tissues of mice with LR induction. CRLM tissues and CRLM-adjacent liver tissues from mice with and without LR induction were subjected to investigating dysregulation of CER metabolism. (A and B) Heatmap illustrating the difference in mRNA levels of CER metabolic enzymes in CRLM-adjacent liver tissues (A) and CRLM tissues (B) between mice with and without LR induction, including *Sptlc1*, *Cerkl*, *Degs1*, *Degs2*, *Cers1*, *Cers2*, *Cers3*, *Cers4*, *Cers5*, *Cers6*, *Cerk*, *Cert*, *Acer2*, *Acer3*, *Asah1*, *Asah2*, *Sphk1*, *Sphk2*, *Sgpp1*, *Sgpp2*, *S1pr1*, *S1pr2*, *S1pr3*, *S1pr4*, *S1pr5*, *Sgpl1*, *Galc*, *Gla*, *Gba1*, *Gba2*, *B4galt6*, *Smpd1*, *Smpd2*, *Smpd3*, *Smpd4*, *Smpd5*, *Enpp7*, *Ugcg*, *Naaa*, *Samd8*, *Sgms1*, *Sgms2*, *Smpd3a*, and *Smpd3b*. (C–E) (C) Immunoblotting of SMPD3 and quantification of protein levels of SMPD3 in CRLM-adjacent liver tissues. (D) Immunostaining of SMPD3 and quantification of SMPD3-positive cells in CRLM-adjacent liver tissues. (E) Immunofluorescent co-staining of HNF4α and SMPD3 in CRLM-adjacent liver tissues. Images in D and E represent results from 1 of 5 pairs of mice in each group. Data in A, B, C, and D were expressed as mean \pm standard deviation, $n = 5$ in each group. * $P < .05$, ** $P < .01$, *** $P < .001$.

was no significant difference in the uptake of LR-Exo and Sham-Exo by metastatic CRC cells in the liver in vivo (Figure 6A and B). We found that the injection of LR-Exo, compared with Sham-Exo, promoted the progression of CRLM with increased weight and territorial expansion of macroscopic CRLM (Figure 7A–F). Notably, *Smpd3*

knockdown substantially augmented the pro-cancer activities of LR-Exo, resulting in more significant increases in the weight and territory of macroscopic CRLM (Figure 7A–F). Examinations of apoptosis by cCASP3 and TUNEL staining demonstrated that *Smpd3* knockdown substantially inhibited the pro-apoptotic activities of the

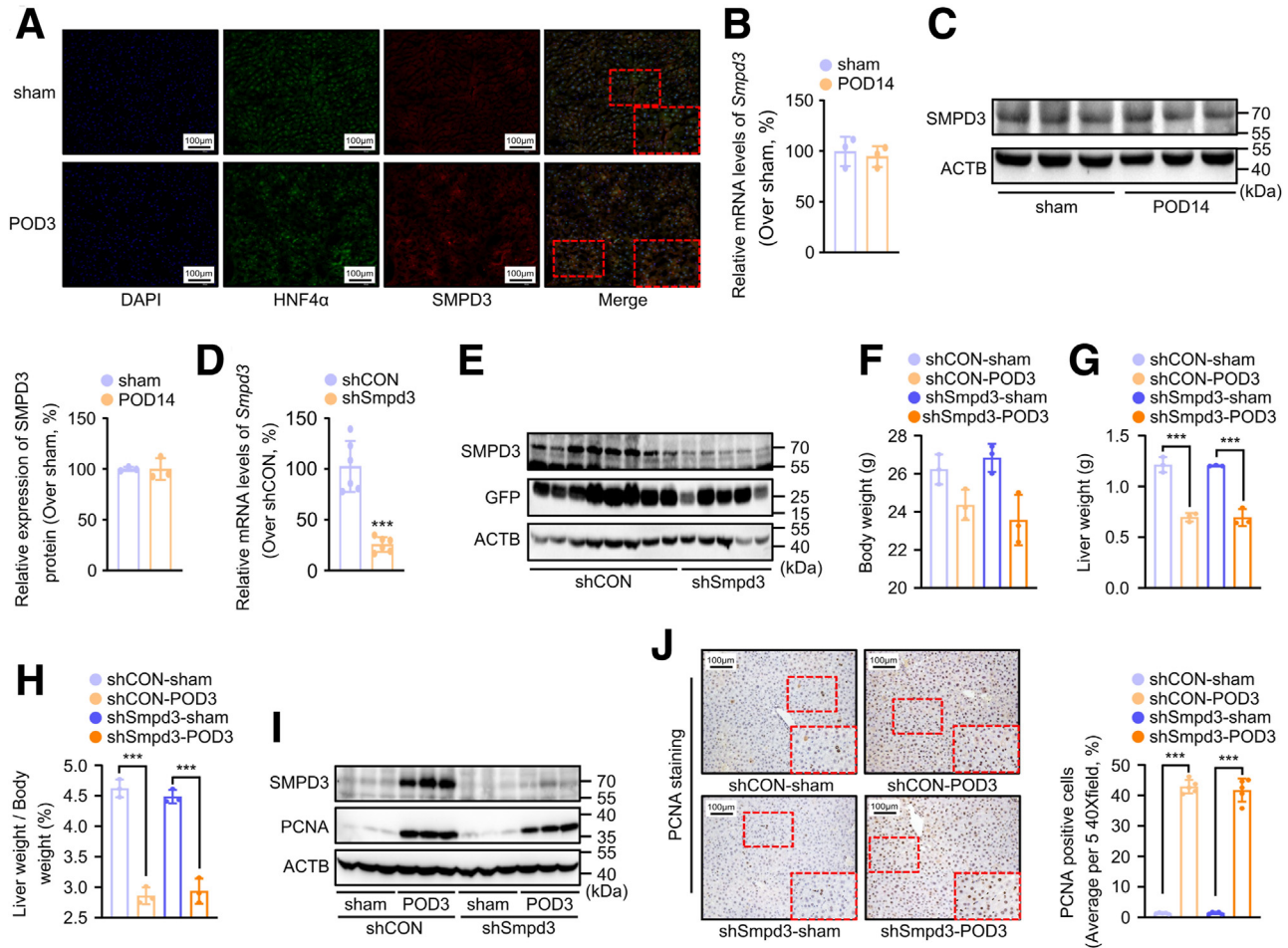


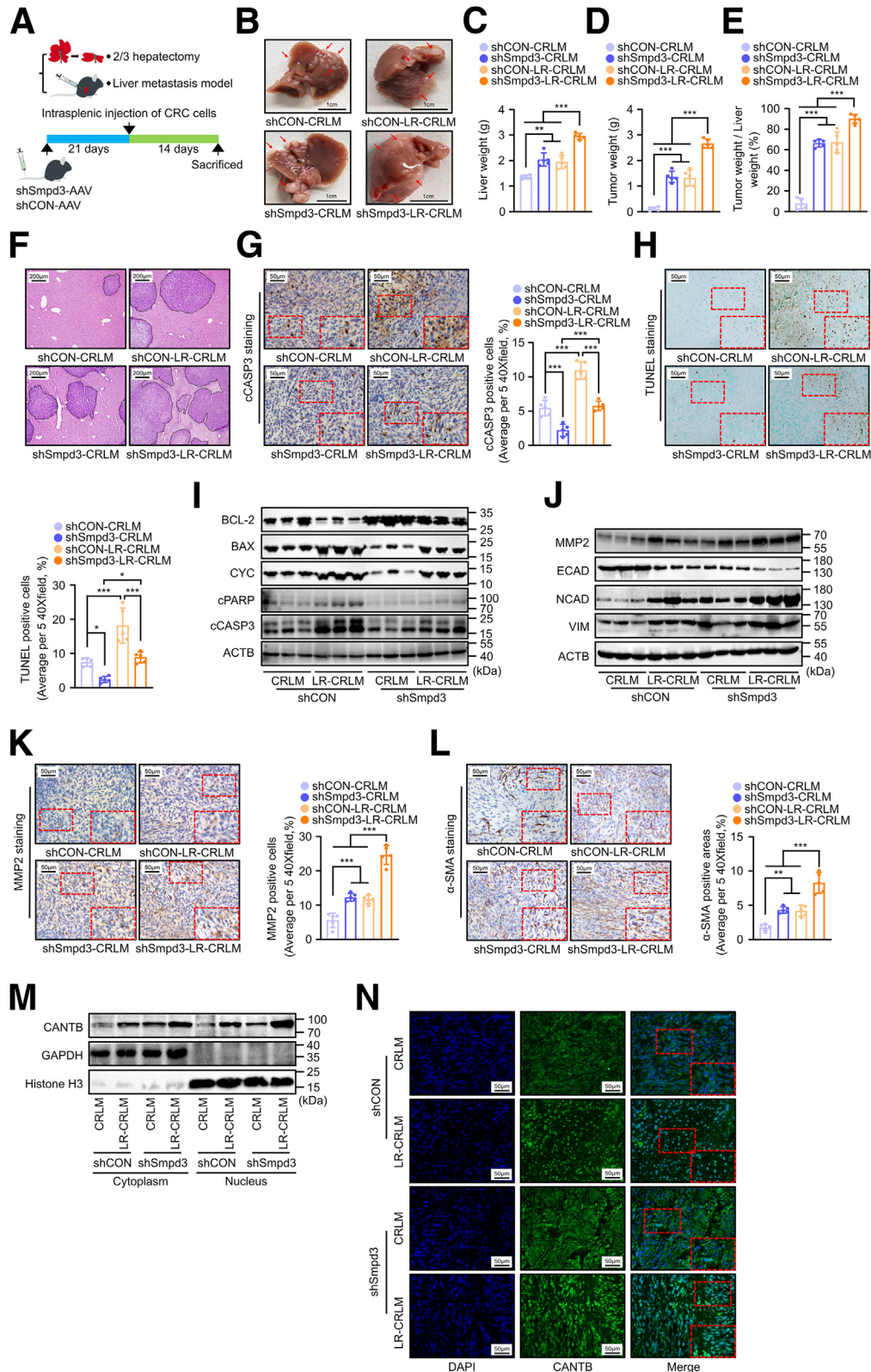
Figure 3. Smpd3 knockdown has no impact on LR in mice. (A–C) Healthy C57BL/6J mice were subjected to 2/3 PH or sham operation. Then liver tissues were harvested at early (postoperative day 3, POD3) and late stages (postoperative day 14, POD14) after PH. (A) Immunofluorescent co-staining of hepatocyte marker HNF4 α and SMPD3 was performed to detect expression of SMPD3 in hepatocytes of sham and POD3 mice. (B) The mRNA levels of *Smpd3* in the liver of sham and POD14 mice. (C) Immunoblotting of SMPD3 on proteins extracted from liver of sham and POD14 mice. (D and E) Hepatic *Smpd3* was knocked down by systemic administration of liver-directed AAV carrying an shSmpd3 vector. *Smpd3* knockdown efficiency was measured at 3 weeks after AAV injection. (D) The mRNA levels of *Smpd3* in the liver of shSmpd3-AAV and shCON-AAV transfected mice. (E) Immunoblotting of SMPD3 and green fluorescent protein on proteins extracted from the liver of shSmpd3-AAV and shCON-AAV transfected mice. (F–J) shSmpd3 and shCON mice were subjected to 2/3 hepatectomy or sham surgery. Then liver tissues were harvested at postoperative day 3 (POD3) and subjected to examination of LR. (F) Mouse body weight. (G) Mouse liver weight. (H) Ratio of liver weight and body weight in mice. (I) Immunoblotting of PCNA and SMPD3 on proteins extracted from liver tissues. (J) Immunostaining of PCNA and quantification of PCNA-positive cells in the liver. Images in A and J represent results from 1 of 3 pairs of mice in each group. Data in D and J were expressed as mean \pm standard deviation, n = 5 in each group. Data in B, C, F, G, and H were expressed as mean \pm standard deviation, n = 3 in each group. ****P* < 0.001.

LR-Exo and Sham-Exo (Figure 7G and H). Mechanistically, injection of LR-Exo promoted apoptosis in CRLM by activating the mitochondrial pathway of apoptosis, indicated by the increased protein levels of BAX, CYC, cPARP, and cCASP3 and the decreased protein levels of BCL-2 in CRLM after the injection of LR-Exo compared with those after injection of Sham-Exo (Figure 7I). *Smpd3* knockdown markedly suppressed the pro-apoptotic activities of LR-Exo and Sham-Exo, indicated by the decreased protein levels of Bax, CYC, cPARP, and cCASP3 and the increased protein levels of BCL-2 in CRLM (Figure 7I), suggesting that *Smpd3* knockdown weakens the pro-apoptotic activities of LR-Exo and Sham-Exo through suppressing the activation of

mitochondrial pathway of apoptosis. Next, we investigated whether SPMD3 also regulated the pro-invasive activities of LR-Exo. Examination of MMP2 and EMT markers demonstrated that injection of LR-Exo exosomes up-regulated MMP2 and promoted EMT in CRC cells in CRLM, indicated by the increased protein levels of MMP2 and EMT makers in CRLM after the injection of LR-Exo compared with those after the injection of Sham-Exo (Figure 7J–L). *Smpd3* knockdown substantially augmented the up-regulation of MMP2 and EMT makers in CRLM treated with LR-Exo (Figure 7J–L). Notably, compared with the exosomes isolated from the knockdown control mice, Sham-Exo from *Smpd3* knockdown mice was also found to

promote CRLM in the normal liver by increasing the invasiveness in metastatic CRC cells (Figure 7J-L). However, the effects of Smpd3 knockdown on increasing the invasiveness

of metastatic CRC cells were more profound in the LR-Exo (Figure 7J-L). These results demonstrate that LR-Exo can conduct the anti-CRLM and pro-CRLM effects of LR



induction on CRLM. Moreover, hepatic SMPD3 plays a critical role in preserving the anti-CRLM activity of LR-Exo by inducing mitochondrial apoptosis and restricting the increase in the invasiveness of metastatic CRC cells.

SMPD3 Controls the LR-Activated Production of Exosomal CER in Hepatocytes to Elevate CER in CRLM

SMPD3 has recently been found to regulate the CER in extracellular vesicles,²⁹ and CER is implicated in attenuating the aggressiveness of various cancers.^{15,17,47,48} Because we consolidated that SMPD3 preserved the anti-CRLM property of LR-derived exosomes, we hypothesized that the up-regulation of SMPD3 in CRLM-adjacent hepatocytes might elevate the levels of CER in CRLM by controlling the production of exosomal CER. To this end, we conducted lipidomics analyses to measure the alteration of CER levels in the CRLM and CRLM-adjacent liver tissues. We found that the levels of CER were significantly increased in CRLM in the remnant liver after PH compared with those in the normal liver, including CER(d18:1/16:0), CER(d18:1/18:0), CER(d18:1/18:1), CER(d18:1/20:0), CER(d18:1/22:0), CER(d18:1/22:1), CER(d18:1/24:0), CER(d18:1/24:1), and total CER (Figure 8A). The levels of CER metabolites, including SPH(d18:1) and S1P(d18:1), in CRLM tissues were not affected by the induction of LR (Figure 8B and C). Moreover, the levels of CER were also increased in the CRLM-adjacent tissues in the remnant liver after PH compared with those in the normal liver, including CER(d18:1/16:0), CER(d18:1/24:1), and total CER (Figure 8D). The levels of CER metabolites, including SPH(d18:1) and S1P(d18:1), in CRLM-adjacent tissues were not affected by the induction of LR (Figure 8E and F). By analyzing the levels of CER in CRLM and CRLM-adjacent tissues of hepatic Smpd3 knockdown mice, we found that hepatic Smpd3 knockdown did not substantially affect the levels of CER in CRLM and CRLM-adjacent liver tissues in the mice without LR induction (Figure 8G and H). However, hepatic Smpd3 knockdown was sufficient to abolish the elevation of CER in CRLM in the remnant liver after PH, including the elevation of CER(d18:1/22:1), CER(d18:1/24:0), CER(d18:1/24:1), and total CER

(Figure 8G). Importantly, hepatic Smpd3 knockdown abolished the elevation of CER in CRLM-adjacent tissues in the remnant liver after PH, including CER(d18:1/22:0), CER(d18:1/24:0), and total CER (Figure 8H). These data suggest that the up-regulation of SMPD3 in CRLM-adjacent hepatocytes contributes to the elevation of CER in the CRLM.

Next, we investigated whether SMPD3 regulated the CER levels in exosomes. Measurements of CER levels in the isolated exosomes demonstrated that the levels of CER were significantly elevated in the LR-Exo compared with the Sham-Exo, including CER(d18:1/18:1), CER(d18:1/22:1), CER(d18:1/24:1), and total CER (Figure 9A). Moreover, hepatic Smpd3 knockdown significantly reduced the levels of CER in the LR-Exo and the Sham-Exo, including CER(d18:1/16:0), CER(d18:1/18:0), CER(d18:1/22:1), CER(d18:1/24:0), CER(d18:1/24:1), and total CER (Figure 9A). By examining the CER levels in CRLM from mice that received exosome injection, we found that injection of LR-Exo significantly increased the levels of CER in CRLM compared with injection of Sham-Exo, including CER(d18:1/16:0), CER(d18:1/18:0), CER(d18:1/18:1), CER(d18:1/20:0), CER(d18:1/24:0), CER(d18:1/24:1), and total CER (Figure 9B). These data confirm that exosomes conduct the intercellular transfer of CER. Notably, hepatic Smpd3 knockdown suppressed the LR-Exo-induced elevation of CER in CRLM more profoundly, including CER(d18:1/18:0), CER(d18:1/20:0), CER(d18:1/22:0), CER(d18:1/24:0), CER(d18:1/24:1), and total CER (Figure 9B). Finally, we used GW4869 to block the SMPD3-mediated exosome production^{24,49} and tested whether the blockage of exosome production affected the CER levels in CRLM. Mice after 2/3 PH or sham surgery were treated with GW4869 and vehicle. The serum samples were first collected from these mice at post-operative day 3 after PH to detect the exosomal makers in the lyophilized serum. We confirmed that induction of LR remarkably increased the production of serum exosomes, and treatment of GW4869 abolished the production of exosomes (Figure 9C). By examining the CER levels in CRLM and LR-CRLM from mice that received the treatment of GW4869, we found that blockage of the SMPD3-mediated exosome generation with GW4869 treatment substantially abolished the elevation of CER in CRLM in the remnant liver after PH

Figure 4. (See previous page). Up-regulation of SMPD3 in LR impedes CRLM by inducing mitochondrial apoptosis and restricting invasiveness of metastatic CRC cells. (A) Schematic diagram depicting experimental design of LR-CRLM model in Smpd3 knockdown mice. CRLM and LR-CRLM models were established in Smpd3 knockdown mice. Liver tissues were harvested at 2 weeks after establishing CRLM and LR-CRLM models. (B–F) Pathology of CRLM in shSmpd3-AAV and shCON-AAV transfected mice with and without LR induction. (B) Morphology of CRLM; arrows indicate CRLM. (C) Mouse liver weight. (D) Mouse macroscopic tumor weight. (E) Ratio of macroscopic tumor weight and liver weight in mice. (F) H&E staining of liver sections; dotted line area indicates area of CRLM. (G–I) Examination on apoptosis in CRLM of shSmpd3-AAV and shCON-AAV transfected mice with and without LR induction. (G) Immunostaining of cCASP3 and quantification of cCASP3-positive cells in CRLM. (H) TUNEL staining and quantification of TUNEL-positive cells in CRLM. (I) Immunoblotting of BCL-2, BAX, CYC, cCASP3, and cPARP on proteins extracted from CRLM tissues. (J–L) Measurement of MMP2 expression and EMT markers in CRLM of shSmpd3-AAV and shCON-AAV transfected mice with and without LR induction. (J) Immunoblotting of MMP2 and EMT markers. (K) Immunostaining of MMP2 and quantification of MMP2-positive cells in CRLM. (L) Immunostaining of α -SMA and quantification of α -SMA-positive areas in CRLM. (M and N) Examination on Wnt/CANTB activation in CRLM of shSmpd3-AAV and shCON-AAV transfected mice with and without LR induction. (M) Immunoblotting of CANTB on proteins extracted from CRLM tissues. (N) Immunostaining of CANTB in CRLM. Images in B, F, G, H, K, L, M, and N represent results from 1 of 5 pairs of mice in each group. Data in C, D, E, G, H, K, and L were expressed as mean \pm standard deviation, n = 5 in each group. *P < 0.05, **P < 0.01, ***P < 0.001.

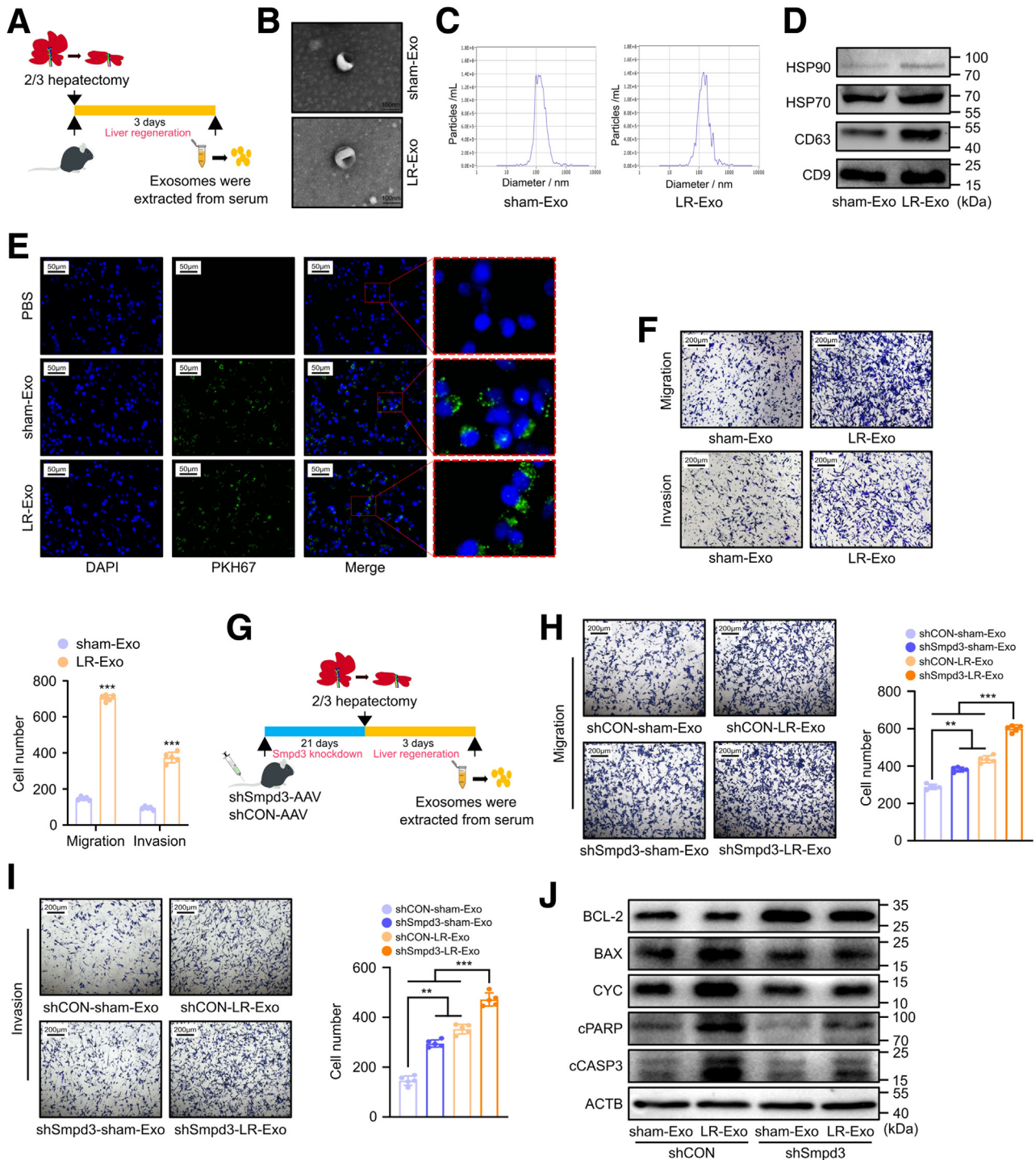


Figure 5. Hepatic SMPD3 retains anti-cancer properties of LR-derived exosomes by maintaining their pro-apoptotic and anti-invasive activities in vitro. (A) Schematic diagram depicting experimental design of exosome extraction. Exosomes were isolated from serum of mice at POD3 after PH (LR-Exo). Exosomes isolated from mice that received sham surgery were used as the vehicle control (sham-Exo). (B–D) Verification of isolated exosomes. (B) Ultrastructure of exosomes observed under transmission electron microscope. (C) NTA analysis of exosome size. (D) Expression of exosome surface markers HSP90, HSP70, CD63, and CD9 measured by Western blot analysis. (E) PKH67-labeled sham-Exo and LR-Exo were uptaken by MC38 cells. (F) Effects of sham-Exo and LR-Exo on migration of invasion of MC38 cells. (G) Schematic diagram depicting experimental design of exosome extraction. Exosomes were isolated from serum of shSmpd3 and shCON mice at POD3 after PH or sham surgery. (H and I) Effects of shSmpd3-Exo and shCON-Exo on migration of invasion of MC38 cells. (J) Examination on apoptosis in MC38 cells with treatment of shSmpd3-Exo and shCON-Exo. Immunoblotting of BCL-2, BAX, CYC, cCASP3, and cPARP on proteins extracted from MC38 cells. Images in B, C, and D represent results from 1 of 5 pairs of mice in each group. Images in E, F, H, I, and J represent results from 3 independent experiments. Data in F, H, and I were expressed as mean ± standard deviation, n = 5 in each group. **P < .01, ***P < .001.

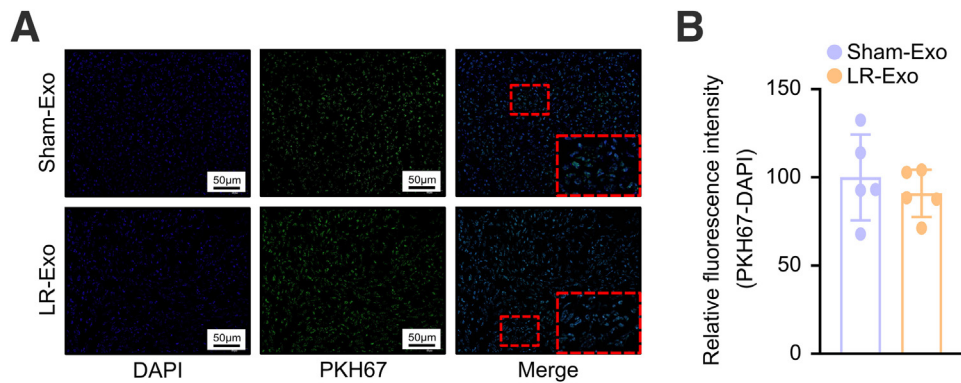


Figure 6. In vivo internalization of Sham-Exo and LR-Exo in CRLM. PKH67-labeled Sham-Exo and LR-Exo were injected into CRLM mice without LR induction. After 30 minutes, CRLM tissues were harvested to examine in vivo internalization of Sham-Exo and LR-Exo. (A and B) Representative images (A) and quantification data (B) of CRLM sections from mice injected with 10 μg Sham-Exo and LR-Exo. Images in A represent results from 1 of 3 pairs of mice in each group. Data in B were expressed as mean \pm standard deviation, $n = 5$ in each group.

(Figure 9D), including the elevation of CER(d18:1/16:0), CER(d18:1/18:0), CER(d18:1/18:1), CER(d18:1/20:0), CER(d18:1/22:0), CER(d18:1/22:1), CER(d18:1/24:0), CER(d18:1/24:1), and total CER (Figure 9D). These data collectively suggest that induction of LR elevates the levels of CER in CRLM by SMPD3-controlled exosome-bound transfer of CER from hepatocytes to metastatic CRC cells.

SMPD3 Controls the Exosome-Bond Intercellular Transfer of CER to Impede the Progression of CRLM in the Context of LR

CER has been implicated in inducing apoptosis and suppressing migration and invasion in various cancer cells.^{20,50–54} Because the induction of LR increased the levels of CER in CRLM via exosome-bound intercellular transfer of CER, we hypothesized that CER might constitute the anti-CRLM properties of LR-derived exosomes by inducing apoptosis and suppressing the invasiveness of CRLM. Thus, we investigated whether the blockage of the SMPD3-mediated exosome-bound intercellular transfer of CER by GW4869 treatment further promoted CRLM in the context of LR. We found that GW4869 treatment indeed promoted the progression of CRLM with increases in territory more profoundly in the liver with LR induction than in the normal liver (Figure 10A–F). Mechanistically, GW4869 treatment attenuated the mitochondrial apoptosis and promoted MMP2 up-regulation and EMT in CRLM more profoundly in the liver with LR induction than in the normal liver (Figure 10G–L). These data consolidate that SMPD3-generated exosomal CER in response to LR impedes the progression of CRLM by promoting apoptosis and reducing the invasiveness in CRLM.

To pinpoint the anti-cancer function of exosomal CER in CRLM in the context of LR, we constructed LipCER to mimic the exosome-bound CER and investigated the anti-CRLM role of LipCER in CRLM in the context of LR. In vitro studies demonstrated that LipCER treatment significantly increased MC38 cell death (Figure 11A and B) and inhibited migration and invasion in MC38 cells (Figure 11C). Next, we investigated the therapeutic effects of LipCER injection in the

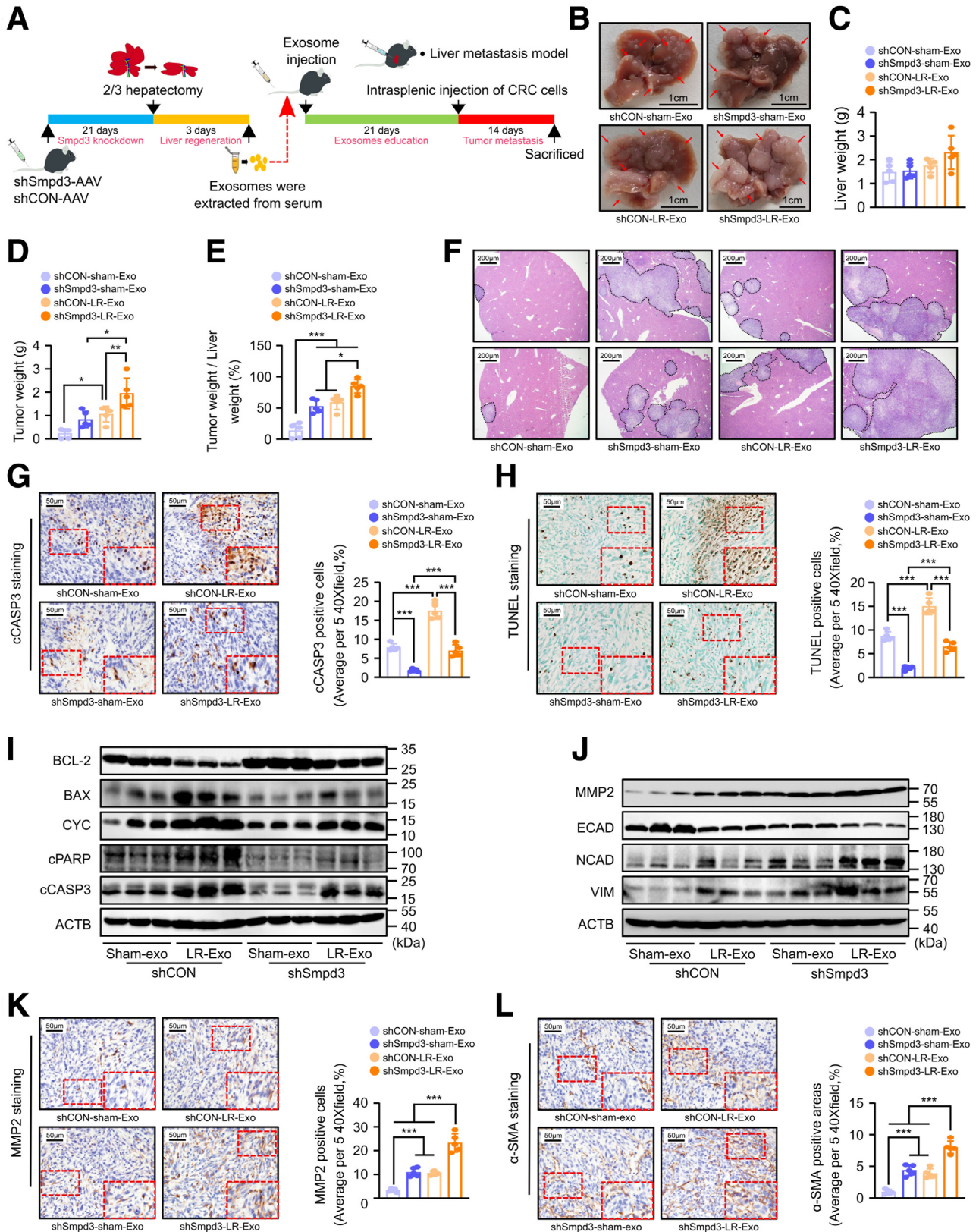
mouse model of CRLM with LR induction. We first found that LipCER injection did not affect the process of LR in mice, including body weight, liver weight, and hepatocellular proliferation (Figure 12A–E). Then, we found that LipCER injection significantly suppressed the progression of CRLM, indicated by decreases in the weight and territory of macroscopic CRLM in the liver with induction of LR (Figure 13A–G). Examinations of apoptosis by cCASP3 and TUNEL staining demonstrated that LipCER injection promoted apoptosis in CRLM in the context of LR with increased apoptotic CRC cells compared with the vehicle injection (Figure 13H and I). Consistently, LipCER injection increased the protein levels of BAX, CYC, cPARP, and cCASP3, while reducing the protein levels of BCL-2 (Figure 13J), suggesting that LipCER injection induces apoptosis by activating the mitochondrial pathway of apoptosis (Figure 13J). Examination of MMP2 and EMT markers demonstrated that LipCER injection markedly down-regulated MMP2 and suppressed EMT in CRC cells in CRLM in the context of LR, indicated by down-regulation of MMP2 and decreased protein levels of EMT markers in CRLM (Figure 13K–M). Mechanistically, LipCER injection significantly decreased CANTB expression in the nuclear fractions in metastatic CRC cells of CRLM in the remnant liver after PH (Figure 13N and O). These results demonstrate that LipCER treatment, which mimics the intercellular transfer of CER, can suppress the progression of CRLM by promoting apoptosis and reducing invasiveness in CRLM. Collectively, these data suggest that the SMPD3-mediated exosome-bound intercellular transfer of CER critically impedes the progression of CRLM in the context of LR by promoting apoptosis and reducing invasiveness in metastatic CRC cells. Thus, SMPD3-produced exosomal CER constitutes a critical anti-CRLM mechanism in the context of LR.

Discussion

Our study reports novel findings regarding the role and mechanism of LR in governing CRLM. Our data demonstrate

that induction of LR by PH results in aggressive CRLM with augmented apoptosis and increased invasiveness. Furthermore, the LR-derived exosomes conduct the bidirectional

regulatory effects of LR on CRLM, including the anti-CRLM of inducing apoptosis and the pro-CRLM effects of increasing invasiveness. Our mechanistic studies reveal that



the up-regulation of SMPD3 in regenerating hepatocytes during early post-hepatectomy stages and in the CRLM-adjacent hepatocytes after CRLM formation serves as a protective mechanism against CRLM in the context of LR. This protective mechanism fosters exosomal CER production, which transfers CER from hepatocytes to metastatic CRC cells to mitigate CRLM by inducing apoptosis and restricting the invasiveness in metastatic CRC cells. Enhancing this defensive mechanism via modulation of SMPD3-mediated exosomal CER generation or supplementation of CER may offer novel therapeutic approaches against CRLM within the LR milieu.

Previous studies provide contradictory results regarding the impact of PH-induced LR on CRLM. Although relevant studies demonstrated that LR promoted the progression of CRLM with increased tumor growth by promoting the proliferation of metastatic CRC cells,^{8,9} Schwarz et al¹² demonstrated that LR could suppress the progression of CRLM. To further elucidate the role of LR in regulating CRLM, our study demonstrates that induction of LR by PH regulates CRLM bidirectionally by augmenting apoptosis and enhancing invasiveness in metastatic CRC cells, resulting in aggressive CRLM (Figure 1). LR is a comprehensive and well-orchestrated process to overcome liver injuries. Emerging studies demonstrate that LR produces both anti-cancer and pro-cancer signaling molecules to regulate cancer biology bidirectionally. In line with this notion, the augmented apoptosis in metastatic CRC cells may represent the protective effect of LR against CRLM, and the increase in invasiveness with up-regulation of MMP2 and EMT in metastatic CRC cells may be considered as the “side effect” of LR on CRLM. Because we observed that induction of LR resulted in aggressive CRLM with increased weight and territory of macroscopic tumor (Figure 1A–E), we concluded that the anti-CRLM machinery of inducing apoptosis is less competitive against the pro-CRLM machinery of increasing the invasiveness, eventually rendering LR to facilitate the progression of CRLM. Enhancing the anti-CRLM machinery or suppressing the pro-CRLM machinery in the process of LR may offer promising strategies to prevent CRLM after PH.

Dysregulation of CER metabolism has been implicated in regulating cancer metastasis and LR.^{34,55,56} CER is generated via the de novo, catabolic, and salvage pathway and degraded by ceramidases to SPH and S1P.¹⁷ The rapid CER generation is mainly catalyzed by sphingomyelinases, which

break down sphingomyelins (SM) to produce CER.³⁸ CER has been implicated in cancer biology as anti-cancer lipid with pro-death activities.^{35,57} Our study demonstrates that induction of LR robustly up-regulates SMPD3 in the CRLM-adjacent hepatocytes (Figure 2A, C, and E) and also in the regenerating liver tissues at the early stage after PH (Figure 3A and I). Notably, in mice without injection of CRC cells, the SMPD3 in hepatocytes was also up-regulated in the regenerating liver at the early stage after hepatectomy but receded at the late stage after hepatectomy (Figure 3B and C). Therefore, we propose that the presence of CRLM may be essential to maintain the up-regulation of SMPD3 in the CRLM-adjacent hepatocytes. Knockdown of *Smpd3* in the liver further augments the pro-CRLM effects of LR by abolishing apoptosis and promoting MMP2 expression and EMT in the metastatic CRC cells (Figure 4G–L), suggesting a protective role of hepatic SMPD3 against CRLM in the context of LR. Mechanistically, we found that SMPD3 might regulate MMP2 expression and EMT by modulating the nuclear translocation of CANTB (Figure 4M and N). Interestingly, we found that knockdown of *Smpd3* also promoted the progression of CRLM in the normal liver (Figure 4B–F) but less profoundly than it did in the remnant liver after PH, suggesting that hepatic SMPD3 plays a more critical role in exerting the anti-CRLM effect in the context of LR than it does in the normal liver. Previous studies reported that the elevation of SMPD3 in the remnant liver after PH was correlated with the proliferation of hepatocytes.^{27,28} However, our study found that hepatic *Smpd3* knockdown had no significant impact on the proliferation of hepatocytes during LR (Figure 3F–J). Thus, the hepatic SMPD3 may not directly regulate hepatocellular proliferation during LR. Besides *Smpd3*, we also found up-regulation of mRNA levels of *Sgpp2*, *Degs1*, *Degs2*, *B4galt6*, and *Smpdl3b* in the CRLM-adjacent-liver tissues (Figure 2A). *Sgpp2* can dephosphorylate S1P into sphingosine,⁵⁸ *Degs1* and *Degs2* catalyze the synthesis of CER,⁵⁹ *B4galt6* catalyzes the synthesis of galactosylceramides,⁶⁰ and *Smpdl3b* involves in the SM catabolic processes.⁶¹ The role of *Sgpp2* in cancer has not yet been reported. *Degs1*, *Degs2*, *B4galt6*, and *Smpdl3b* have been implicated in regulating cell survival, metastasis, immunity, and cancer.^{62–64} The potential role of these genes in regulating CRLM after induction of LR still needs further investigation.

Figure 7. (See previous page). Hepatic SMPD3 retains anti-CRLM properties of LR-derived exosomes by maintaining their pro-apoptotic and anti-invasive activities. (A) Schematic diagram depicting exosome injection. Healthy mice were subjected to the education mouse model using LR-Exo and Sham-Exo for 21 days. Then MC38 cells were intrasplenically injected into educated mice without LR induction. Then liver tissues were harvested after another 14 days injection of exosomes. (B–F) Pathology of CRLM in mice treated with LR-Exo and Sham-Exo. (B) Morphology of CRLM; arrows indicate CRLM. (C) Mouse liver weight. (D) Mouse macroscopic tumor weight. (E) Ratio of macroscopic tumor weight and liver weight in mice. (F) H&E staining of liver sections; dotted line area indicates area of CRLM. (G–I) Examination on apoptosis in CRLM of mice treated with LR-Exo and Sham-Exo. (G) Immunostaining of cCASP3 and quantification of cCASP3-positive cells in CRLM. (H) TUNEL staining and quantification of TUNEL-positive cells in CRLM. (I) Immunoblotting of BCL-2, BAX, CYC, cCASP3, and cPARP on proteins extracted from CRLM tissues. (J–L) Measurement of MMPs expression and evaluation of EMT in CRLM of mice treated with LR-Exo and Sham-Exo. (J) Immunoblotting of MMP2 and EMT markers. (K) Immunostaining of MMP2 and quantification of MMP2-positive cells in CRLM. (L) Immunostaining of α -SMA and quantification of α -SMA-positive areas in CRLM. Images in B, G, H, K, and L represent results from 1 of 5 pairs of mice in each group. Data in C, D, E, G, H, K, and L were expressed as mean \pm standard deviation, n = 5 in each group. **P* < .05, ***P* < 0.01, ****P* < 0.001.

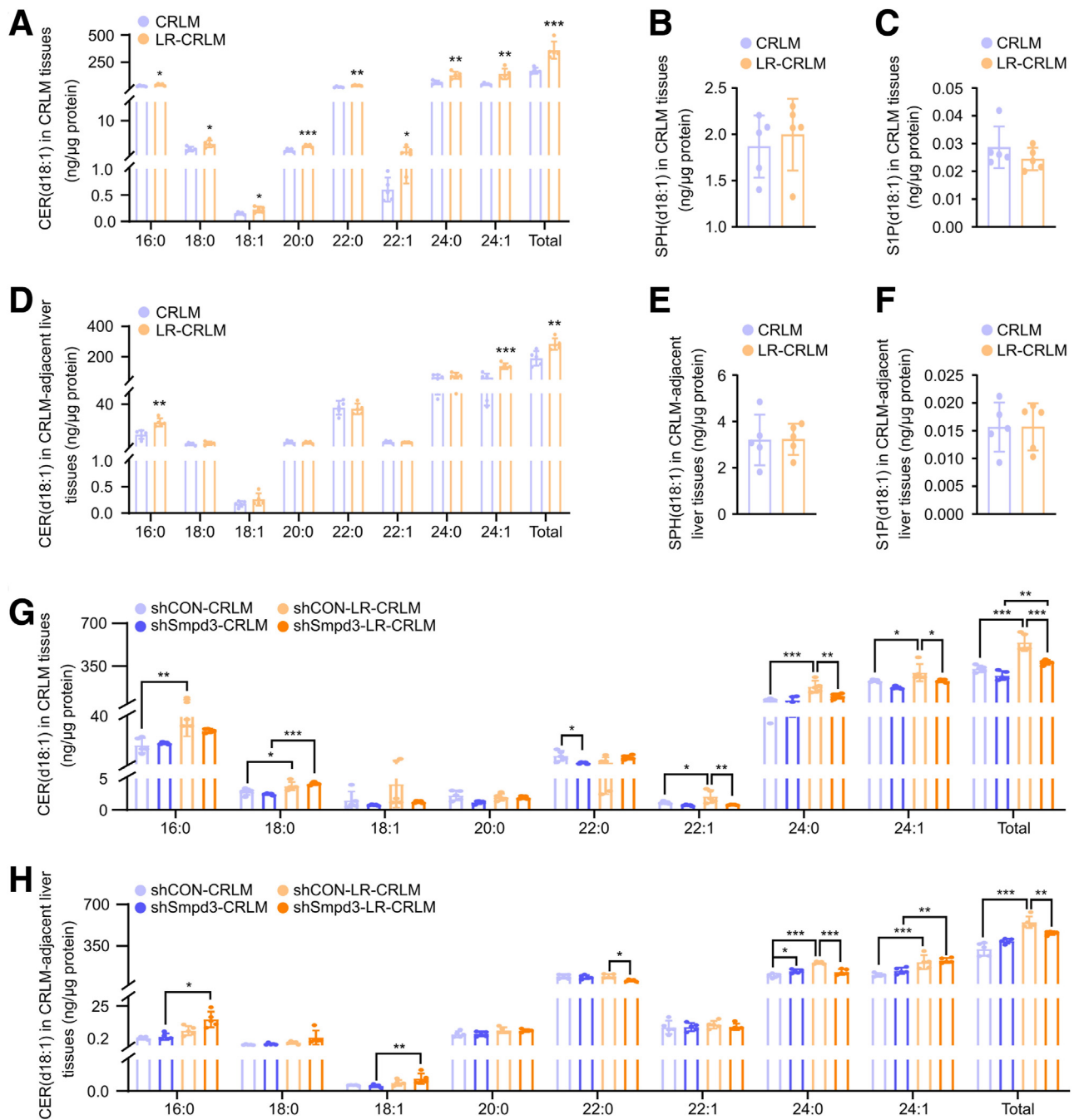


Figure 8. Up-regulation of SMPD3 in CRLM-adjacent hepatocytes contributes to elevation of CER in CRLM. (A–C) Levels of CER(d18:1) (A) and its metabolites in CRLM tissues from mice with and without LR induction including SPH(d18:1) (B) and S1P(d18:1) (C). (D–F) Levels of CER(d18:1) (D) and its metabolites in CRLM-adjacent liver tissues from mice with and without LR induction including SPH(d18:1) (E) and S1P(d18:1) (F). (G and H) Levels of CER(d18:1) in CRLM (G) and CRLM-adjacent liver tissues (H) from shSmpd3-AAV and shCON-AAV transduced mice with and without LR induction. Data in A, B, C, D, E, F, G, and H were expressed as mean \pm standard deviation, $n = 5$ in each group. * $P < .05$, ** $P < .01$, *** $P < .001$.

SMPD3 is known to regulate cancer malignancy by regulating the levels of CER.^{65,66} In this study, we found that induction of LR resulted in elevations of CER in the CRLM and CRLM-adjacent liver tissues (Figure 8A and D), and knockdown of Smpd3 in the liver abolished the LR-induced elevation of CER in the CRLM and CRLM-adjacent liver tissues (Figure 8G and H). Moreover, by screening the CER

metabolic enzymes in CRLM, we found that the mRNA levels of CER metabolic enzymes were not significantly different between the CRLM in the normal liver and those in the remnant liver after PH (Figure 2B), suggesting that the elevation of CER in CRLM in response to LR is more likely dependent on the uptake of extrinsic CER. In the extracellular environment, CER is enriched in exosomes, and the

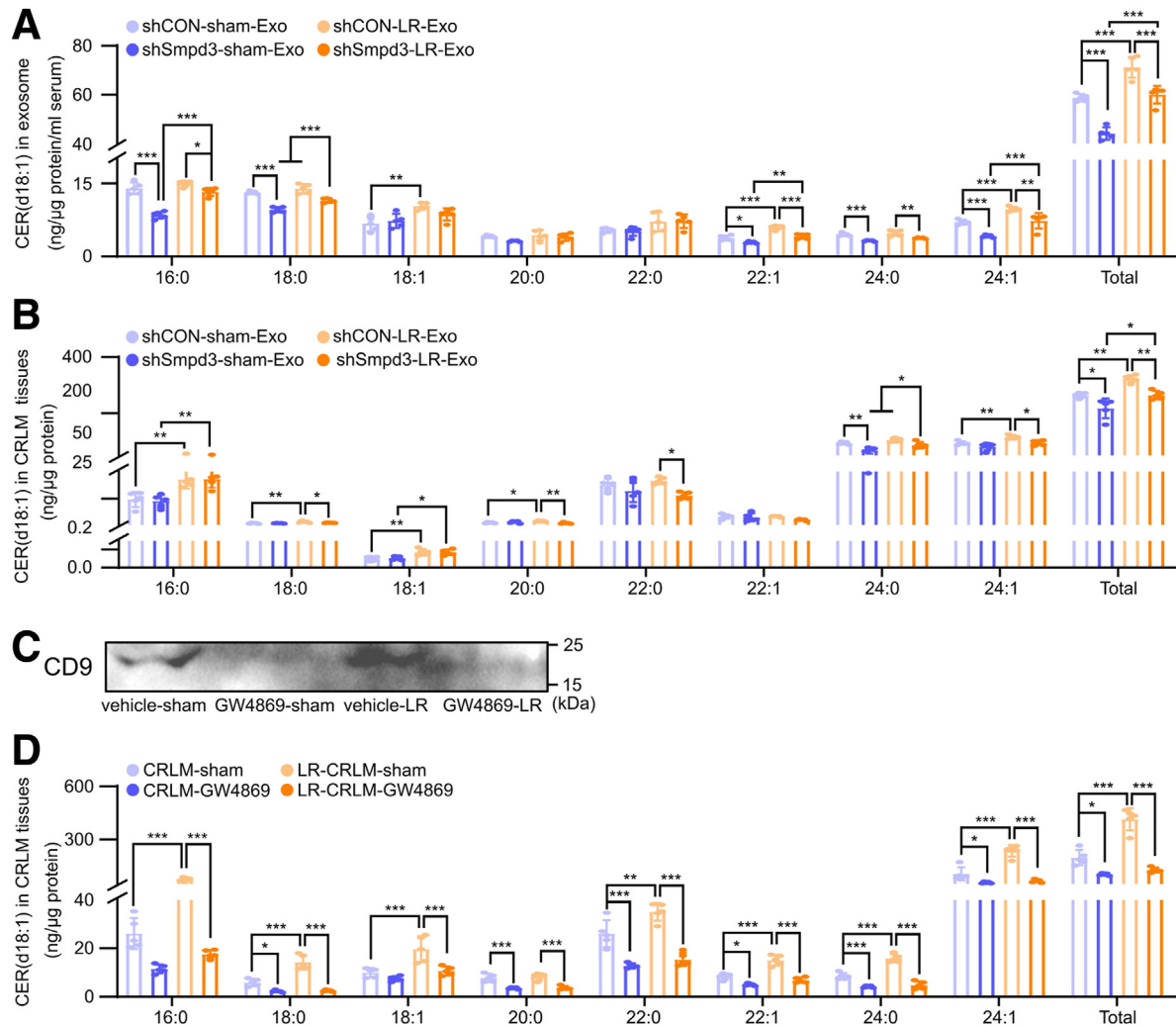


Figure 9. SMPD3 controls LR-activated production of exosomal CER in hepatocytes to elevate CER in CRLM. (A) Levels of CER(d18:1) in serum exosomes isolated from shSmpd3-AAV and shCON-AAV transfected mice with and without LR induction. (B) Levels of CER(d18:1) in CRLM tissues of mice after Sham-Exo and LR-Exo treatment. (C) GW4869 was used to block SMPD3-mediated exosome production. Serum samples were collected from mice at POD3 after PH with and without GW4869 treatment. Expression of exosome surface marker CD9 in lyophilized serum was detected by Western blot analysis. (D) Levels of CER(d18:1) in CRLM tissues of mice after GW4869 treatment. Images in C represent results from 1 of 5 pairs of mice in each group. Data in A, B, and D were expressed as mean \pm standard deviation, $n = 5$ in each group. * $P < .05$, ** $P < .01$, *** $P < .001$.

SPMD3-generated CER is essential for forming and releasing exosomes.²⁴ Meanwhile, exosomes conduct intercellular communication via the delivery of cell metabolites to modulate the biology of target cells.^{67,68} Zietzer et al²⁹ recently demonstrated that CER could be transferred intercellularly via extracellular vesicles. In line with these findings, we showed that LR-derived exosomes conducted the anti-CRLM and pro-CRLM effects by promoting apoptosis and increasing invasiveness, respectively (Figure 7G–L). Knockdown of hepatic SMPD3 was found to reduce the content of CER in exosomes isolated from normal mice and abolish the LR-induced increase of CER in exosomes isolated from mice with LR (Figure 9A), suggesting that SPMD3 plays a crucial role in controlling the CER content in exosomes and up-regulation of SPMD3 mediates the increase in CER in exosomes in response to LR. By

blockage of exosome generation using a pharmacologic inhibitor of SPMD3, we found that CER levels were decreased in the CRLM in the remnant liver after PH (Figure 9D). These data highlight the critical role of exosomes in conducting the intercellular transfer of SMPD3-produced CER from hepatocytes to metastatic CRC cells. Because cancer cells are recognized for their enhanced capacity to internalize exosomes compared with soluble molecules,^{69,70} the function of the exosomal CER in regulating CRLM may be more significant than the soluble CER. Nonetheless, the potential function of soluble CER in regulating CRLM within LR still needs further investigation.

CER is a group of bioactive lipids that activate various anti-cancer signaling pathways in various cancers.^{14,15,18,54,71,72} Several studies have implicated CER as the critical pro-death lipid that activates the

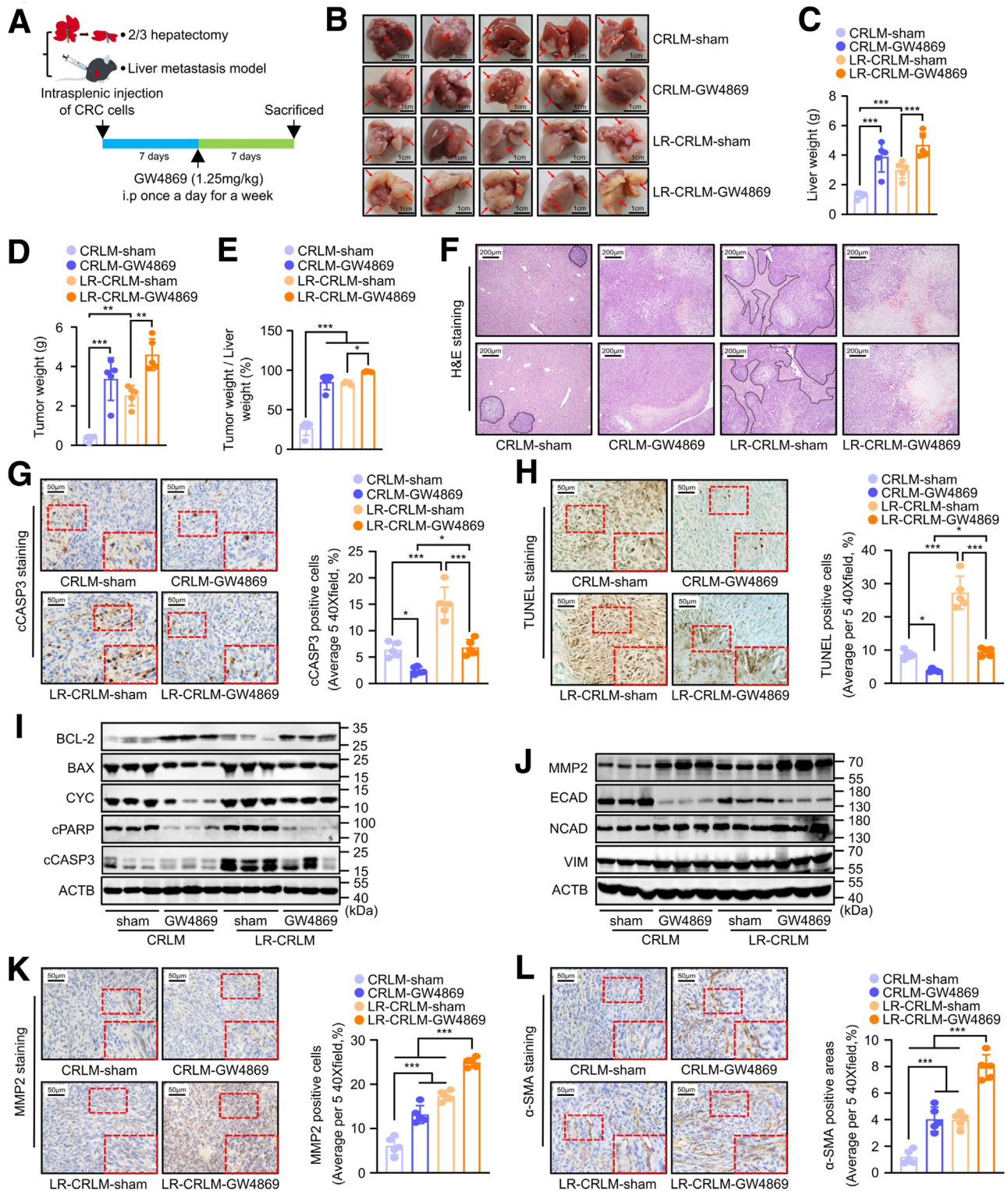


Figure 10. GW4869 treatment promotes CRLM by inhibiting mitochondrial apoptosis and increasing invasiveness of metastatic CRC cells. (A) Schematic diagram depicting experimental design. One week after establishing CRLM and LR-CRLM models, mice were treated with GW4869 once a day for another week. Then liver tissues were harvested for examination. (B–F) Pathology of CRLM. (B) Morphology of CRLM; arrows indicate CRLM. (C) Mouse liver weight. (D) Mouse macroscopic tumor weight. (E) Ratio of macroscopic tumor weight and liver weight in mice. (F) H&E staining of liver sections; dotted line area indicates area of LR-CRLM. (G–I) Examination on apoptosis in CRLM. (G) Immunostaining of cCASP3 and quantification of cCASP3-positive cells in CRLM. (H) TUNEL staining and quantification of TUNEL-positive cells in CRLM. (I) Immunoblotting of BCL-2, BAX, CYC, cPARP, and cCASP3 on protein extracted from CRLM tissues. (J–L) Measurement of MMP2 expression and evaluation of EMT in CRLM. (J) Immunoblotting of MMP2 and EMT markers. (K) Immunostaining of MMP2 and quantification of MMP2-positive cells in CRLM. (L) Immunostaining of α -SMA and quantification of α -SMA-positive areas in CRLM. Images in G, H, K, and L represent results from 1 of 5 pairs of mice in each group. Data in C, D, E, G, H, K, and L were expressed as mean \pm standard deviation, n = 5 in each group. * $P < .05$, *** $P < .001$.

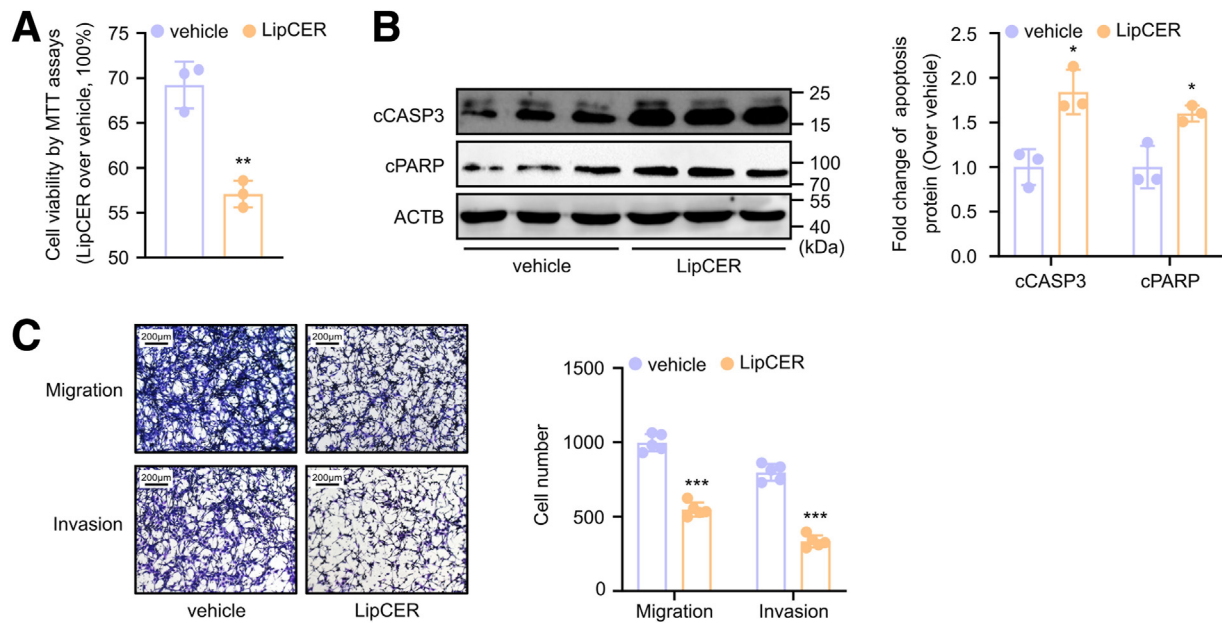


Figure 11. LipCER induces apoptosis and inhibits migration/invasion in MC38 cells. LipCER (10 μ mol/L) was added to culture medium of MC38 cells for 36 hours. Then viability of MC38 cells was evaluated by MTT assays. Cell proteins were extracted for evaluation of expression levels of apoptosis makers. Effects of LipCER on migration of invasion of MC38 cells were tested by using Transwell assays. (A) Cell viability of MC38 cells with and without LipCER treatment. (B) Evaluation of expression levels of apoptosis makers in MC38 cells with and without LipCER treatment. (B) Immunoblotting of cCASP3 and cPARP and quantifications of protein levels of cCASP3 and cPARP in MC38 cells. (C) Effects of LipCER on migration and invasion of MC38 cells. Images in C represent results from 3 independent experiments. Data in A and B are expressed as mean \pm standard deviation, $n = 3$ in each group. Data in C were expressed as mean \pm standard deviation, $n = 5$ in each group. * $P < .05$, ** $P < .01$, *** $P < .001$.

mitochondrial pathway of apoptosis and suppresses the signaling pathways involved in MMP expression and EMT in CRC cells.^{19,20,35,73} Consistently, our data demonstrate that

activation of the SPMD3-produced exosomal CER induces mitochondrial apoptosis and restricts the increase in invasiveness with suppression of MMP2 expression and EMT in

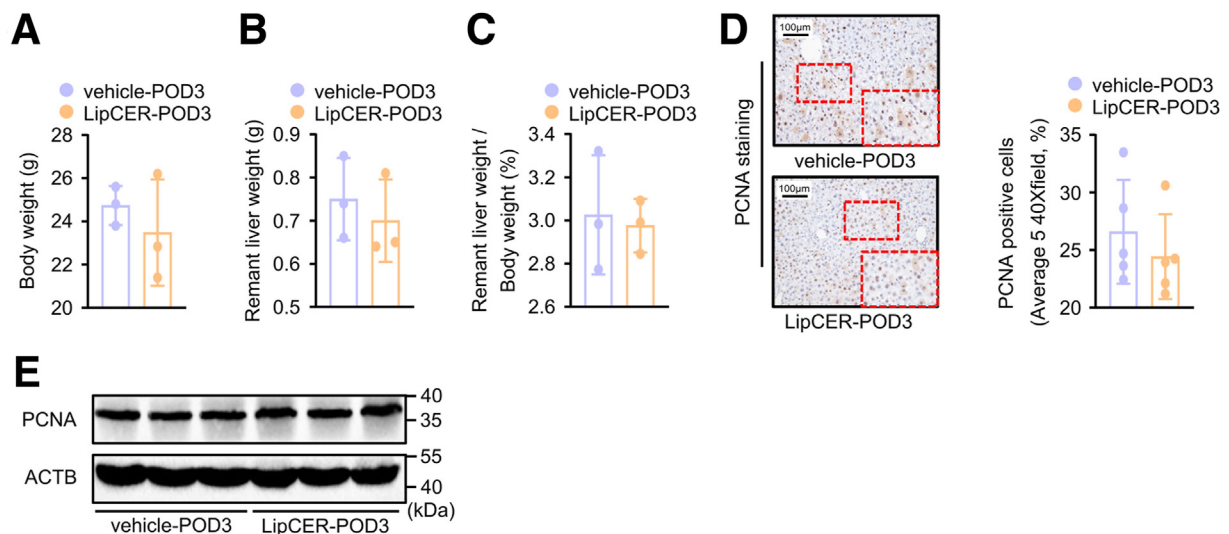
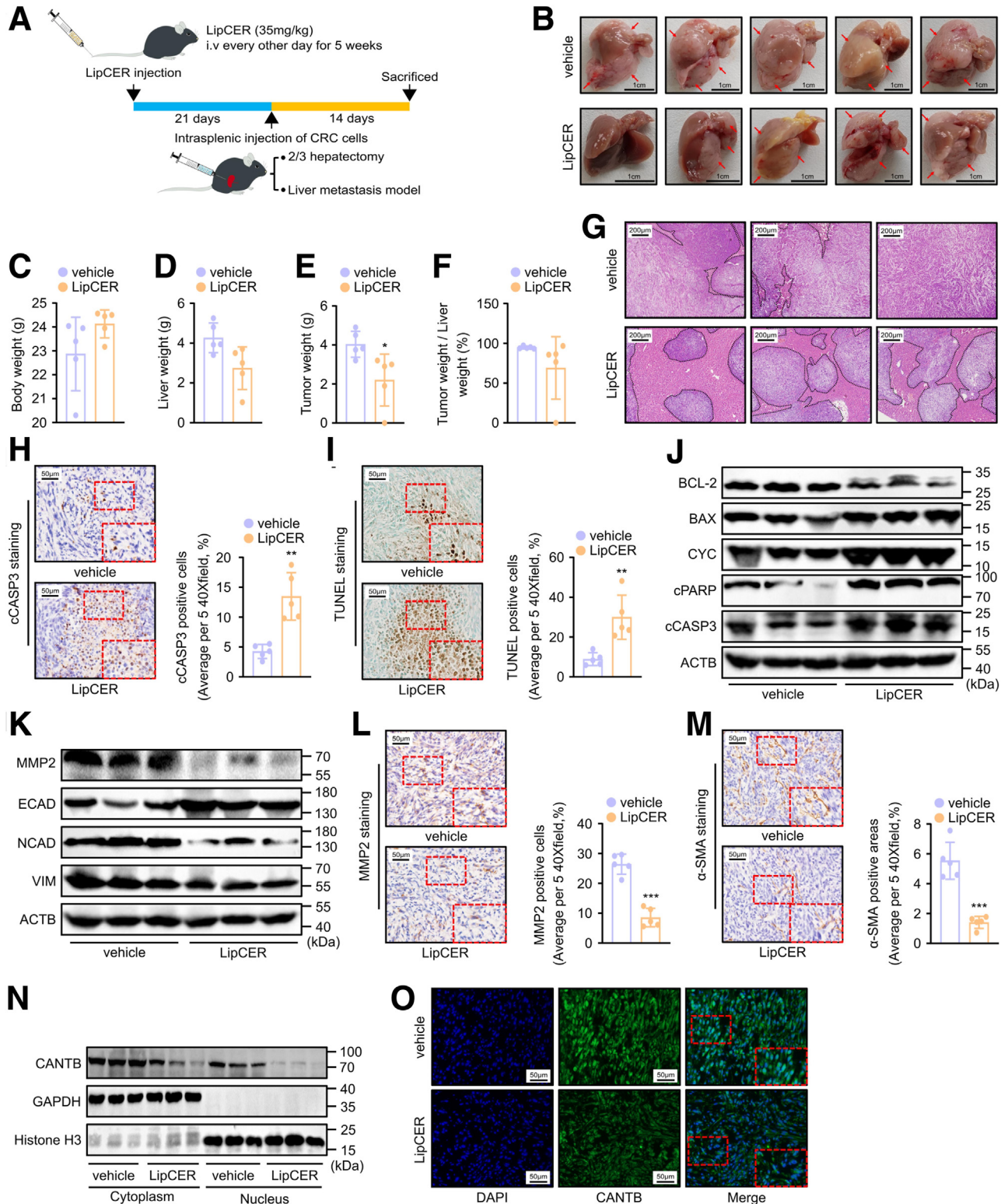


Figure 12. LipCER injection has no significant impact on LR in mice. C57BL/6J mice were treated with 2/3 hepatectomy. Then LipCER or vehicle liposomes were injected via the tail vein every other day at a dose of 35 mg/kg body weight. Liver tissues were harvested 3 days after the operation for examination. (A–E) Examination of LR in mice. (A) Mouse body weight. (B) Weight of the remnant liver. (C) Ratio of remnant liver weight and body weight in mice. (D) Immunostaining of PCNA and quantification of PCNA-positive cells in the mouse liver. (E) Immunoblotting of PCNA on protein extracted from liver tissues. Images in D represent results from 1 of 3 pairs of mice in each group. Data in A, B, and C are expressed as mean \pm standard deviation, $n = 3$ in each group. Data in D are expressed as mean \pm standard deviation, $n = 5$ in each group.

target CRC cells (Figure 7G-L). Although LR harbors SPMD3-produced exosomal CER as anti-CRLM machinery, we still observed that induction of LR indeed promoted the progression of CRLM (Figure 1A-E) and that inhibition of exosomal CER generation further promoted CRLM after

induction of LR (Figures 7B-F and 10B-F). Importantly, treatment of LipCER was found to substantially suppress CRLM by inducing apoptosis and reducing invasiveness in CRLM (Figure 13H-M). These data collectively suggest that the exosomal CER at physiological levels only impedes LR



from further promoting the progression of CRLM without eradicating CRLM; however, upon augmenting CER levels through exogenous administration, it may become sufficient to eradicate CRLM. Notably, we found that the supplement of LipCER did not impact the normal process of LR (Figure 12A–E). This might be attributed to the up-regulation of ceramidase activity to prevent the accumulation of CER in the regenerating liver.²⁸ Because LipCER has been implicated as an anti-cancer therapeutic agent,²¹ these findings offer a promise of using CER as a therapeutic option to prevent the recurrence of CRLM after PH.

In conclusion, our work provides new insight into the anti-CLRM mechanism by which induction of LR impedes the progression of CRLM. These discoveries offer new strategies for manipulating the SMPD3-mediated CER metabolism to prevent CRLM in the regenerating liver and present the potential for using CER as a therapeutic approach to prevent CRLM recurrence after PH.

Materials and Methods

Mice

Six-week-old male C57BL/6J mice were purchased from the animal experiment center of Southern Medical University (Guangzhou, China) and maintained in a specific pathogen-free (SPF) environment. All animal experiments were approved by the Institutional Animal Care and Use Committee of Nanfang Hospital Southern Medical University.

Mice Experiments

Mouse 2/3 hepatectomy was performed as described by Mitchell and Willenbring.⁷⁴ The mice CRLM model was performed as described by Yu et al.⁷⁵ Briefly, 8-week-old C57BL/6J mice were anesthetized by isoflurane inhalant, and their abdominal cavities were opened to expose the liver and spleen. For the liver metastasis model, mice were injected intrasplenically with 5×10^5 MC38 cells in 100 μ L phosphate-buffered saline, followed by splenectomy at 3 minutes after injections. Then mice of the LR-CRLM group were subjected to 2/3 hepatectomy by removing the left lateral and median lobes. Mice of the control (CRLM) group were subjected to intrasplenic injection of MC38 cell without 2/3

liver resection. At 14 days after surgery, mice were killed, and tissues were collected. For in vivo Smpd3 knockdown, liver-directed AAVs,⁷⁶ type 8 AAVs carrying an shRNA targeting Smpd3 gene (shSmpd3; 5'-ccATTCTTTCAGTCACGATTT-3'), or a control shRNA (shCON; 5'-CGCTGAGTACTTCGAAATGTC-3') with a green fluorescent protein reporter gene (Jikai Biology, Shanghai, China) were injected into the tail vein of normal mice via a 28-gauge needle. Smpd3 knockdown efficiency was examined by real-time PCR analyses and Western blotting assay. For blockage of the SMPD3-mediated exosome generation with GW4869 treatment, GW4869 (Selleck, Houston, TX) was dissolved in saline with 2.5% dimethyl sulfoxide, and the same volume of 2.5% dimethyl sulfoxide saline was used as vehicle control. One week after establishing the CRLM model, the mice were administered GW4869 intraperitoneally (1 mg/kg) every 24 hours for 7 days. Mice were killed, and tissues were collected after a 7-day treatment. For exosome treatment, serum exosomes were isolated from the Smpd3 knockdown and their control mice 3 days after 2/3 hepatectomy without CRLM modeling. Twenty μ g exosomes were injected into wild-type C57BL/6J mice through the tail vein before establishing the CRLM model every other day for 21 days. Mice were killed at 14 days after establishing the CRLM model, and tissues were collected. For LipCER treatment, LipCER (35 mg/kg body weight) or vehicle was injected into wild-type C57BL/6J mice via the tail vein before and after establishing the CRLM model every other day for 3 weeks and 2 weeks, respectively. Mice were killed 2 weeks after establishing the CRLM model, and tissues were collected.

Quantitative Real-Time Polymerase Chain Reaction

Total RNA was extracted from liver tissues, CRLM tissues, and CRLM-adjacent liver tissues using TriZol reagent. mRNA was reversely transcribed to cDNA by EV M-MLV RT Premix (Accurate Biology; Changsha, China). Quantitative PCR analyses were performed on an ABI Prism 7000 sequence detection system (Thermo, RINGOES, NJ). Relative mRNA levels of the indicated genes were calculated using the delta-delta CT method. β -Actin was used as a reference gene. Primer sequences used to amplify specific gene fragments are listed in Table 1.

Figure 13. (See previous page). LipCER slows LR-CRLM by inducing mitochondrial apoptosis and restricting increase in invasiveness of metastatic CRC cells. (A) Schematic diagram depicting LipCER administration. LipCER or vehicle nanoliposomes were injected via the tail vein every other day for 2 weeks at dose of 35 mg/kg body weight before and after establishing the LR-CRLM model. (B–G) Pathology of LR-CRLM of mice treated with and without LipCER treatment. (B) Morphology of LR-CRLM; arrows indicate LR-CRLM. (C) Mouse body weight. (D) Mouse liver weight. (E) Mouse macroscopic tumor weight. (F) Ratio of macroscopic tumor weight and liver weight in mice. (G) H&E staining of liver sections; dotted line area indicates the area of LR-CRLM. (H–J) Examination on apoptosis in LR-CRLM of mice treated with and without LipCER treatment. (H) Immunostaining of cCASP3 and quantification of cCASP3-positive cells in LR-CRLM. (I) TUNEL staining and quantification of TUNEL-positive cells in LR-CRLM. (J) Immunoblotting of BCL-2, BAX, CYC, cCASP3, and cPARP on protein extracted from LR-CRLM tissues. (K–M) Measurement of MMP2 expression and evaluation of EMT in LR-CRLM of mice treated with and without LipCER treatment. (K) Immunoblotting of MMP2 and EMT markers in LR-CRLM. (L) Immunostaining of MMP2 and quantification of MMP2-positive cells in LR-CRLM. (M) Immunostaining of α -SMA and quantification of α -SMA-positive areas in LR-CRLM. (N and O) Examination on Wnt/CANTB activation in LR-CRLM of mice treated with and without LipCER treatment. (N) Immunoblotting of CANTB on proteins extracted from LR-CRLM tissues. (O) Immunostaining of CANTB in LR-CRLM. Images in H, I, L, M, and O represent results from 1 of 5 pairs of mice in each group. Data in C, D, E, F, H, I, L, and M were expressed as mean \pm standard deviation, n = 5 in each group. * $P < .05$, ** $P < .01$, *** $P < .001$.

Table 1. Primers for Real-Time PCR Assays

Gene	qPCR primer sequence
<i>Actb</i>	5'-GATGTATGAAGGCTTTGGTC-3' 5'-TGTGCACTTTTATTGGTCTC-3'
<i>Sptlc1</i>	5'-TACGAGGCTCCAGCATACC-3' 5'-TCAGAACGCTCCTGCAACT-3'
<i>Cerkl</i>	5'-GAAGCATGGCTCTTAGGGT-3' 5'-CTCCTCCTGTGGGCTGTAT-3'
<i>Degs1</i>	5'-CTACTCCTATTATGGGCTCTG-3' 5'-CTCACTTGCATCTTCTCA-3'
<i>Degs2</i>	5'-ACTTTGTGGCTGAGCATTAT-3' 5'-AGTCATCCAGTGGCAGGT-3'
<i>Cers1</i>	5'-CTCATTGCCTCTTCTACGC-3' 5'-CAGCTGCACATCGCTGAC-3'
<i>Cers2</i>	5'-TCATCCCTTCTCAGTATTGGT-3' 5'-ATCCTTTCGCTTGACATCAG-3'
<i>Cers3</i>	5'-GGCGATTACATTTTACTTGCTG-3' 5'-GGTCATATGCCCATGGTTTG-3'
<i>Cers4</i>	5'-ACCCTGAATTTGCCCTGTA-3' 5'-CTTGAAGTCCTTGCCTTG-3'
<i>Cers5</i>	5'-GATGCTGTTTGAGCGATT-3' 5'-TGGGTTCCACCTTATTGAC-3'
<i>Cers6</i>	5'-TGTGCCATAGCCCTCAAC-3' 5'-CTCCGAACATCCAGTCC-3'
<i>Cerk</i>	5'-ATCTCCACGGGACAATAAA-3' 5'-GGCCATACAGGGCTTTC-3'
<i>Cert</i>	5'-TTTGATGAATGCCGTTTG-3' 5'-ATAGCCACTCGCTCCAGAC-3'
<i>Asah1</i>	5'-AATAACACTTGGGTTGTAC-3' 5'-TAGGATACCCAGATAACCAC-3'
<i>Asah2</i>	5'-AGAGAGAGCAAGGTATTCTTC-3' 5'-ACTATTCAAAAAGTGGTTGC-3'
<i>Acer2</i>	5'-GTGTGGCATTCTCATCTG-3' 5'-TAAGGGACACCAATAAAAGC-3'
<i>Acer3</i>	5'-GATTCACTGAGGAACCTTCG-3' 5'-AGAGAACTTCACTTTTGGC-3'
<i>Sphk1</i>	5'-ACAGACCATCCAAAGGTAGTTT-3' 5'-CTCTATTCTGTGCTCAGTGTGC-3'
<i>Sphk2</i>	5'-GTACTCATGTTGGGCATCTT-3' 5'-CATACTCCACTAACTCCCA-3'
<i>Sgpp1</i>	5'-GAGCAACTTGCCGCTCTACTA-3' 5'-GGTCGAGATTCCAGATCCAGAA-3'
<i>Sgpp2</i>	5'-AAGATTGGTTGTGATATGGTT-3' 5'-GATGAGGAGGGTGAAGGAGAT-3'
<i>S1pr1</i>	5'-TCCTGGTTCTGGCTGTGC-3' 5'-TGGGCTCTTGAATTTGC-3'
<i>S1pr2</i>	5'-ATGGGCGGCTTATACTCAGAG-3' 5'-GCGCAGCACAAAGATGATGAT-3'
<i>S1pr3</i>	5'-GTTCTTCTGATTGGGATGTG-3' 5'-AATGGCGGTGAAGATACTGA-3'
<i>S1pr4</i>	5'-CTACTCCAAGGGCTATGTGC-3' 5'-TGGCTCGGACCACTCTAA-3'
<i>S1pr5</i>	5'-CTTGGCCATTGCTTTAGAGC-3' 5'-AGTAAATCCTTGCATAGAGCGC-3'
<i>Sgp1</i>	5'-GAACCGACCTCCTCAAGCT-3' 5'-TCATACACCCAGACTATCAGC-3'
<i>Galc</i>	5'-CCGATTTCTTCTTCTGCT-3' 5'-GGTTCAATATGCGACTCCAA-3'

Table 1. Continued

Gene	qPCR primer sequence
<i>Gla</i>	5'-ACCCTTTCATAAGCCCAATT-3' 5'-GGTCCAGCGACTTCAACAA-3'
<i>Gba1</i>	5'-TCGTGTTAAACCGATCTTCG-3' 5'-TGAATGGAGTAGCCAGGTGA-3'
<i>Gba2</i>	5'-CGTCCTTTGCCCTCGTC-3' 5'-TGCCACCCTCCACTCATC-3'
<i>B4galt6</i>	5'-AAACAGCGGCTGGAATT-3' 5'-TGGCCTCTTTGAAACCC-3'
<i>Smpd1</i>	5'-GCCTGCAAAGTCTTATTAC-3' 5'-CACCACATCGTCCCTCAAAG-3'
<i>Smpd2</i>	5'-GCCCAGTTCATCCACCAC-3' 5'-CCTCAGTCTCAACGAAAGC-3'
<i>Smpd3</i>	5'-TCATGGACGTGGCCTATC-3' 5'-ACCTGCACCTTGAGAAACAG-3'
<i>Smpd4</i>	5'-GGAATCTCCGATGCCTACA-3' 5'-ATCATTGGACCACTTGGGT-3'
<i>Smpd5</i>	5'-CATCACCTACCGCAGAGTAC-3' 5'-TCCGTGAGTCCAGCAA-3'
<i>Enpp7</i>	5'-CGGCAAATACATCGAGAACC-3' 5'-CTCTGGATACCGAGCGTGGC-3'
<i>Ugcg</i>	5'-GCTTCGTGCTCTTCGTGG-3' 5'-TTGCCTTCTGTTGAGGTGT-3'
<i>Naaa</i>	5'-CCCAAGGCCATATTTACCA-3' 5'-CAGTCTACATAGCCAACAAAA-3'
<i>Samd8</i>	5'-CAGACCTACCCACCACTCC-3' 5'-TAGCACAGAATCAGGCCAC-3'
<i>Sgms1</i>	5'-GGTCGTCCATGAACGAGTA-3' 5'-TGAATAGCCAGAGTCCATCAA-3'
<i>Sgms2</i>	5'-TGGTATTGGTTGGTTATGG-3' 5'-CGGGCACAGGTAACGTAGTG-3'
<i>Smpd3a</i>	5'-CCTTTGCTGCCTACTGGTT-3' 5'-ATTTGCGCCTTTAGATGAA-3'
<i>Smpd3b</i>	5'-TATCAACTCGTCTTGTATGCC-3' 5'-GAGTTGGTCAAGCGTTCC-3'
<i>MMP2</i>	5'-TGACTTCTTGGATCGGGTCG-3' 5'-AAGCACACATCAGATGACT-3'
<i>MMP3</i>	5'-ACATGGAGACTTTGTCCCTTTG-3' 5'-TTGGCTGAGTGGTAGAGTCCC-3'
<i>MMP7</i>	5'-CTGCCACTGTCCAGGAAG-3' 5'-GGGAGAGTTTTCCAGTCATGG-3'
<i>MMP8</i>	5'-CAACATTGCTTTCGTCTCAAGAG-3' 5'-GCATGGGCAAGGATTCCATT-3'
<i>MMP9</i>	5'-TGCTGGAGATTCGACTTGAAGTC-3' 5'-TGAGTCCAGGCACACCA-3'
<i>MMP10</i>	5'-GAGCCACTAGCCATCCTGG-3' 5'-CTGAGCAAGATCCATGCTTGG-3'
<i>MMP11</i>	5'-CCACTACTTTTCACTGAGGTG-3' 5'-CGTCAAACGGCAAGTTGTCAC-3'
<i>MMP12</i>	5'-CTGCTCCCATGAATGACAGTG-3' 5'-AGTTGCTTCTAGCCCAAAGAAC-3'
<i>MMP13</i>	5'-TGTTTGCAGAGCACTACTTAAA-3' 5'-CAGTCCACTCTAAGCCAAAGAAA-3'
<i>MMP14</i>	5'-ACCCACACACAACGCTCAC-3' 5'-GCCTGTCACTTGTAAACCATAGA-3'

Hematoxylin-Eosin Staining

Tumor and liver tissues were embedded in paraffin blocks and sectioned after being fixed and treated with alcohol series. Sections were stained with hematoxylin-eosin for histology examination.

Immunohistochemistry Staining and TUNEL Assay

Liver sections and tumor sections were prepared as described above, and immunohistochemistry staining was performed using a VECTASTAIN Elite ABC Kit (Vector, Burlingame, CA) and an M.O.M. (Mouse on mouse) Immunodetection Kit (Vector) according to the manufacturer's instructions. Sections subjected to immunohistochemistry staining with antibodies against CD31 (Abcam, Cambridge, MA), SMPD3 (Santa Cruz Biotechnology, Santa Cruz, CA), MMP2 (Cell Signaling Technology, Danvers, MA), cCASP3 (Cell Signaling Technology), proliferating cell nuclear antigen (PCNA) (Cell Signaling Technology), and alpha-smooth muscle actin (α -SMA) (Cell Signaling Technology). The information on the primary antibodies is shown in Table 2. The sections were counterstained with hematoxylin. Positively stained cells were enumerated in 5 random fields per section in a 40 \times field of view under

the Intelligently Designed Microscope (Olympus, Shinjuku, Tokyo, Japan) in a blind manner. TUNEL assays were performed using a TACS-XL In Situ Apoptosis Detection DAB Kit (Trevigen, Gaithersburg, MD) according to the manufacturer's instructions. Methyl green was used for counterstaining. TUNEL-positive cells were enumerated in 5 random fields per section in a 40 \times field of view in a blind manner.

Immunofluorescence Assay

Liver sections and tumor sections were fixed in 4% paraformaldehyde for 10 minutes, blocked with phosphate-buffered saline buffer containing 5% bovine serum albumin, and then incubated with antibodies at 4 $^{\circ}$ C overnight. Anti-hepatocyte nuclear factor 4 α antibody (Bioss, Beijing, China) was used to stain hepatocytes, anti-SMPD3 (Santa Cruz Biotechnology, Santa Cruz, CA) was used to detect the expression of SMPD3 in cells, and anti-CANTB (Santa Cruz Biotechnology) was used to detect the expression of CANTB in metastatic CRC cells nucleus, followed by incubation with secondary antibody at room temperature for 1 hour, and the nuclear was counterstained with diaminophenylindole. Alexa Fluor 488-conjugated antibody (ZSGB-BIO, Beijing, China) and Alexa Fluor 594-conjugated antibody (ZSGB-

Table 2. Primary and Secondary Antibodies for Immunostaining and Immunoblotting

Name	Species	Supplier	Catalogue no.
SMPD3	Mouse	Santa Cruz Biotechnology	sc-166637
MMP2	Rabbit	Cell Signaling Technology	87809
PCNA	Rabbit	Cell Signaling Technology	13110S
Bcl-2	Rabbit	Affinity	AF6139
Bax	Rabbit	Cell Signaling Technology	5023
Hsp70	Rabbit	Abcam	ab181606
Hsp90	Rabbit	Abcam	ab203126
CD9	Rabbit	Proteintech	20597-1-AP
CD63	Rabbit	Abcam	ab217345
Cytochrome C	Rabbit	Abcam	ab133504
N-cadherin	Rabbit	Cell Signaling Technology	13116T
E-cadherin	Rabbit	Cell Signaling Technology	3195T
β -Catenin	Rabbit	Cell Signaling Technology	8480T
Vimentin	Rabbit	Cell Signaling Technology	5744T
α -SMA	Rabbit	Cell Signaling Technology	19245S
Cleaved-caspase 3	Rabbit	Cell Signaling Technology	9664
HNF4 α	Rabbit	Bioss	bs-3828R
CD31	Rabbit	Abcam	ab28364
Histong3 H3	Rabbit	Abcam	ab1791
GAPDH	Rabbit	Abcam	ab8245
Cleaved-PARP	Rabbit	Cell Signaling Technology	5625S
β -Actin	Rabbit	Cell Signaling Technology	AP0060
GFP	Rabbit	Abcam	ab6556
Anti-rabbit IgG HRP		Cell Signaling Technology	7074
Anti-mouse IgG HRP		Cell Signaling Technology	7076
Alexa Fluor 488-conjugated antibody	Rabbit	ZSGB-BIO	ZF-0511
Alexa Fluor 594-conjugated antibody	Mouse	ZSGB-BIO	ZF-0513

BIO) were used as secondary antibodies. The co-stained liver resections were analyzed using an Intelligently Designed Microscope (Olympus).

Western Blotting

Proteins were extracted from MC38 cells, liver tissues, CRLM tissues, CRLM-adjacent tissues, and exosomes by a lysis buffer (50 mmol/L Tris, 1% NP40, 0.25% deoxycholic acid sodium salt, 150 mmol/L NaCl, 1 mmol/L EGTA), and protein concentrations were determined using a bicinchoninic acid protein determination kit (Thermo Scientific, Waltham, MA) according to the manufacturer's instructions. Western blot analyses were performed with antibodies against SMPD3 (Santa Cruz Biotechnology), MMP2 (Cell Signaling Technology), cCASP3 (Cell Signaling Technology), cPARP (Cell Signaling Technology), BCL-2 (Affinity, Changzhou, Jiangsu, China), BAX (Cell Signaling Technology), cytochrome C (CYC) (Abcam), heat shock protein 90 (Abcam), heat shock protein 70 (Abcam), CD63 (Abcam), CD9 (Proteintech, Guangzhou, China), N-cadherin (NCAD) (Cell Signaling Technology), vimentin (VIM) (Cell Signaling Technology), E-cadherin (ECAD) (Cell Signaling Technology), CANTB (Cell Signaling Technology), CD31 (Abcam), GAPDH (Abcam), Histone3 H3 (Abcam), and β -Actin (ACTB) (Cell Signaling Technology). ACTB was used as a loading control. The information on these primary antibodies is listed in Table 2.

Targeted Lipidomics

Lipids were extracted from exosomes, CRLM tissues, and CRLM-adjacent liver tissues using an alkaline methyl tert-butyl ether extraction method as described by Matyash et al.⁷⁷ with slight modifications. Briefly, MeOH (225 μ L, 4°C) was added to the homogenates of exosomes and tissues. After sonication and vortexing, the internal standards (Avanti Polar Lipids, Birmingham, AL) and 750 μ L methyl tert-butyl ether (4°C) were added. The mixture was incubated in a Thermomixer Comfort at 650 rpm for 1 hour at 4°C. Afterward, 188 μ L water was added, and the samples were centrifuged at 10,000g for 10 minutes at 4°C. Then, 600 μ L of the upper organic layer was transferred to another tube and dried under a continuous stream of nitrogen to obtain lipid extracts (1 L/min N₂ at 25°C). The dried lipid extracts were resuspended in 100 μ L of 30% mobile phase B (IPA/ACN, 9/1 [v/v], 0.1 % formic acid, 10 mmol/L ammonium formate, and 5 μ mol/L phosphoric acid) and stored at -80°C before further analysis. After the removal of the interphase, proteins were precipitated from the lower layer by adding 903 μ L MeOH. Samples were stored at -80°C for 4 hours to precipitate protein. Protein pellets were collected after centrifugation at 19,803g for 30 minutes at 4°C and stored in 1% sodium dodecyl sulfate, 150 mmol/L NaCl, 50 mmol/L Tris (pH 7.8) solution at -80°C. The protein content for lipid normalization was quantified by BCA. Lipid standards were obtained from Avanti Polar Lipids, including CER(d18:1/6:0), CER(d18:1/16:0), CER(d18:1/18:0), CER(d18:1/18:1), CER(d18:1/20:0), CER(d18:1/22:0), CER(d18:1/24:0), CER(d18:1/24:1), SPH(d18:1), and S1P(d18:1).

Exosome Isolation and Identification

Isolation and purification of exosomes from mouse serum were performed as described⁴² with slight modifications. Briefly, mouse serum was centrifuged at 2000g for 30 minutes and then at 10,000g for 30 minutes at 4°C, followed by filtration through a 0.45- μ m filter to remove any possible large extracellular vesicles and particles. Exosomes were pelleted by ultracentrifugation at 120,000g for 70 minutes. Exosomes were washed with sterilized phosphate-buffered saline and purified by ultracentrifugation at 120,000g for 70 minutes. Exosomes were resuspended in phosphate-buffered saline. Purified exosomes were observed with a transmission electron microscope (Hitachi, Chiyoda Ward, Tokyo, Japan). The size and number of exosomes were measured by nanoparticle tracking analysis (NTA) (NanoFCM, Xiamen, China). The total protein concentration of isolated exosomes was determined by BCA assays. The presence of exosomes was verified by detecting the protein levels of exosomal markers including CD9, CD63, HSP90, and HSP70.

LipoCER Preparation

LipoCER preparation was performed as described by Tagaram et al.²³ Briefly, lipids including aliquots of 1,2-dioleoyl-sn-glycero-3-phosphocholine (Avanti Polar Lipids), 1,2-dioleoyl-sn-glycero-3-phosphoethanolamine (Avanti Polar Lipids), 1,2-distearoyl-sn-glycero-3-phosphoethanolamine-N-(methoxy (polyethylene glycol)-2000) (Avanti Polar Lipids), C8-ceramide-1-succinyl [methoxy (polyethylene glycol)-750] (Avanti Polar Lipids), and CER(d18:1/6:0) (Avanti Polar Lipids) dissolved in chloroform (CHCl₃) were combined in a 3.75:1.75:0.75:0.75:3 molar ratio. Combined lipids were dried under nitrogen gas and resuspended in 0.9% sterile NaCl solution at 60°C. After rehydration, the resulting solution was subjected to vortex mixing and sonicated, followed by quickly extruded at 60°C by passing the solution at least 10 times through 100-nm polycarbonate filters in an Avanti Polar Lipids Mini-Extruder (Avanti Polar Lipids). Nanoliposome solutions were stored at 4°C until use. Vehicle liposomes were prepared in a similar manner, excluding CER(d18:1/6:0).

Cell Culture

The murine CRC cell line MC38 was purchased from Type Culture Collection of the Chinese Academy of Sciences (Shanghai, China) and was cultured in Dulbecco modified Eagle medium supplemented with 10% fetal bovine serum (Gibco) in a humidified incubator at 37°C with 5% CO₂. Exosomes (40 μ g/mL) were added to the culture medium, and after incubation at 37°C, 5% CO₂ for 36 hours, the cells were collected.

Exosomes Up-Taking Fluorescence Assay

Exosomes were labeled using PKH67 green fluorescent cell linker kit (BestBio, Shanghai, China) according to the manufacturer's instructions. For in vitro exosome up-taking, PKH67-labeled exosomes were incubated with MC38 for 24 hours. For in vivo exosome up-taking, liver sections of

exosome-treated mice were fixed in 4% paraformaldehyde for 10 minutes, and the nuclear was counterstained with DAPI. Exosomes up-taking was observed using the Intelligently Designed Microscope (Olympus) and Inversion Microscope (Olympus).

3-(4,5-Dimethylthiazol-2-yl)-2,5 Diphenyl Tetrazolium Assay

MC38 cells were treated with LipoCER (10 $\mu\text{mol/L}$) and vehicle liposomes at 37°C, 5%CO₂ for 36 hours. MC38 cells were incubated with 3-(4,5-dimethylthiazol-2-yl)-2,5 diphenyl tetrazolium (Merck-Calbiochem, Burlington, MA) solution (5 mg/mL) for 2 hours. Then, lysis buffer (1 mmol/L HCL and 10% Triton X-100 in isopropanol) was added, and plates were incubated at room temperature and gently shaken at 70 rpm for 30 minutes to lysate the cells and elute 3-(4,5-dimethylthiazol-2-yl)-2,5 diphenyl tetrazolium dye. The absorbance was then measured at 590 nm using a multi-mode microplate reader (Molecular Devices, Silicon Valley, CA).

Cell Migration and Invasion Assay

The effect of exosome and LipCER on the migration and invasion of CRC cells was determined using Transwell 24-well plates (8- μm pores; Corning). For cell invasion assays, the upper chambers with 8- μm pores were first pre-coated with 500 ng/mL Matrigel solution (BD Biosciences) and incubated for 4 hours at 37°C. Then, cancer cells (1 \times 10⁵ cells/well) were seeded in the upper chambers in serum-free medium. Meanwhile, the lower chambers were loaded with Dulbecco modified Eagle medium containing 10% fetal bovine serum. Exosome (40 $\mu\text{g/mL}$), LipCER (10 $\mu\text{mol/L}$), and vehicle liposomes (10 $\mu\text{mol/L}$) were added to the upper chambers. After incubation at 37°C, 5% CO₂ for 36 hours, the upper chambers were scratched and immersed, washed with phosphate-buffered saline, fixed with 4% paraformaldehyde, stained with 0.1% crystal violet, and imaged by Inversion Microscope (Olympus). The cell migration assay was performed as above without Matrigel coating.

Statistical Analysis

Statistical analyses were performed with SPSS 20.0 (IBM, Armonk, NY). Statistical significance was determined using Student *t* test or one-way analysis of variance as appropriate, and *P* value <.05 (bilateral) was statistically significant.

References

1. Tauriello DV, Calon A, Lonardo E, et al. Determinants of metastatic competency in colorectal cancer. *Mol Oncol* 2017;11:97–119.
2. The 150 most important questions in cancer research and clinical oncology series: questions 6-14—edited by Chinese Journal of Cancer. *Chin J Cancer* 2017;36:33.
3. Rahbari NN, Birgin E, Bork U, et al. Anterior approach vs conventional hepatectomy for resection of colorectal liver metastasis: a randomized clinical trial. *JAMA Surg* 2021;156:31–40.
4. Mao R, Zhao JJ, Bi XY, et al. A postoperative scoring system for post-hepatectomy early recurrence of colorectal liver metastases. *Oncotarget* 2017; 8:102531–102539.
5. Michalopoulos GK, Bhushan B. Liver regeneration: biological and pathological mechanisms and implications. *Nat Rev Gastroenterol Hepatol* 2021;18:40–55.
6. Riddiough GE, Fifis T, Muralidharan V, et al. Searching for the link: mechanisms underlying liver regeneration and recurrence of colorectal liver metastasis post partial hepatectomy. *J Gastroenterol Hepatol* 2019; 34:1276–1286.
7. Slooter GD, Marquet RL, Jeekel J, et al. Tumour growth stimulation after partial hepatectomy can be reduced by treatment with tumour necrosis factor alpha. *Br J Surg* 1995;82:129–132.
8. Krause P, Flikweert H, Monin M, et al. Increased growth of colorectal liver metastasis following partial hepatectomy. *Clin Exp Metastasis* 2013;30:681–693.
9. Harun N, Nikfarjam M, Muralidharan V, et al. Liver regeneration stimulates tumor metastases. *J Surg Res* 2007;138:284–290.
10. Panis Y, Nordlinger B, Delelo R, et al. Experimental colorectal liver metastases: influence of sex, immunological status and liver regeneration. *J Hepatol* 1990; 11:53–57.
11. Hamm A, Hidding S, Mokry T, et al. Postoperative liver regeneration does not elicit recurrence of colorectal cancer liver metastases after major hepatectomy. *Surg Oncol* 2020;35:24–33.
12. Schwarz L, Nicol L, Francois A, et al. Major hepatectomy decreased tumor growth in an experimental model of bilobar liver metastasis. *HPB (Oxford)* 2020;22: 14801489.
13. Christophi C, Harun N, Fifis T. Liver regeneration and tumor stimulation: a review of cytokine and angiogenic factors. *J Gastrointest Surg* 2008;12:966–980.
14. Moro K, Nagahashi M, Gabriel E, et al. Clinical application of ceramide in cancer treatment. *Breast Cancer* 2019;26:407–415.
15. Taniguchi M, Okazaki T. Role of ceramide/sphingomyelin (SM) balance regulated through “SM cycle” in cancer. *Cell Signal* 2021;87:110119.
16. Murray M, Hraiki A, Bebawy M, et al. Anti-tumor activities of lipids and lipid analogues and their development as potential anticancer drugs. *Pharmacol Ther* 2015; 150:109–128.
17. Hannun YA, Obeid LM. Sphingolipids and their metabolism in physiology and disease. *Nat Rev Mol Cell Biol* 2018;19:175–191.
18. Ogretmen B, Hannun YA. Biologically active sphingolipids in cancer pathogenesis and treatment. *Nat Rev Cancer* 2004;4:604–616.
19. Zhang XF, Li BX, Dong CY, et al. Apoptosis of human colon carcinoma HT-29 cells induced by ceramide. *World J Gastroenterol* 2006;12:3581–3584.
20. de Araujo JR, Eich C, Jorquera C, et al. Ceramide and palmitic acid inhibit macrophage-mediated epithelial-

- mesenchymal transition in colorectal cancer. *Mol Cell Biochem* 2020;468:153–168.
21. Kester M, Bassler J, Fox TE, et al. Preclinical development of a C6-ceramide NanoLiposome, a novel sphingolipid therapeutic. *Biol Chem* 2015;396:737–747.
 22. Li G, Liu D, Kimchi ET, et al. Nanoliposome C6-ceramide increases the anti-tumor immune response and slows growth of liver tumors in mice. *Gastroenterology* 2018;154:1024–1036.e9.
 23. Tagaram HR, Divittore NA, Barth BM, et al. Nanoliposomal ceramide prevents in vivo growth of hepatocellular carcinoma. *Gut* 2011;60:695–701.
 24. Trajkovic K, Hsu C, Chiantia S, et al. Ceramide triggers budding of exosome vesicles into multivesicular endosomes. *Science* 2008;319:1244–1247.
 25. Taniguchi M, Nagaya S, Yuyama K, et al. Ceramide metabolism regulated by sphingomyelin synthase 2 is associated with acquisition of chemoresistance via exosomes in human leukemia cells. *Int J Mol Sci* 2022;23.
 26. Lin M, Liao W, Dong M, et al. Exosomal neutral sphingomyelinase 1 suppresses hepatocellular carcinoma via decreasing the ratio of sphingomyelin/ceramide. *FEBS J* 2018;285:3835–3848.
 27. Albi E, Magni MP. Chromatin neutral sphingomyelinase and its role in hepatic regeneration. *Biochem Biophys Res Commun* 1997;236:29–33.
 28. Zabielski P, Baranowski M, Zendzian-Piotrowska M, et al. Partial hepatectomy activates production of the pro-mitotic intermediates of the sphingomyelin signal transduction pathway in the rat liver. *Prostaglandins Other Lipid Mediat* 2007;83:277–284.
 29. Zietzer A, Jahnke AL, Bulic M, et al. Activation of neutral sphingomyelinase 2 through hyperglycemia contributes to endothelial apoptosis via vesicle-bound intercellular transfer of ceramides. *Cell Mol Life Sci* 2021;79:48.
 30. Kessenbrock K, Plaks V, Werb Z. Matrix metalloproteinases: regulators of the tumor microenvironment. *Cell* 2010;141:52–67.
 31. Latil M, Nassar D, Beck B, et al. Cell-type-specific chromatin states differentially prime squamous cell carcinoma tumor-initiating cells for epithelial to mesenchymal transition. *Cell Stem Cell* 2017;20:191–204.e5.
 32. Li T, Guo H, Song Y, et al. Loss of vinculin and membrane-bound β -catenin promotes metastasis and predicts poor prognosis in colorectal cancer. *Mol Cancer* 2014;13:263.
 33. Jagadish N, Parashar D, Gupta N, et al. A-kinase anchor protein 4 (AKAP4) a promising therapeutic target of colorectal cancer. *J Exp Clin Cancer Res* 2015;34:142.
 34. Sun H, Sun S, Chen G, et al. Ceramides and sphingosine-1-phosphate mediate the distinct effects of M1/M2-macrophage infusion on liver recovery after hepatectomy. *Cell Death Dis* 2021;12:324.
 35. Yun SH, Park ES, Shin SW, et al. Stichoposide C induces apoptosis through the generation of ceramide in leukemia and colorectal cancer cells and shows in vivo anti-tumor activity. *Clin Cancer Res* 2012;18:5934–5948.
 36. Zhou W, Woodson M, Sherman MB, et al. Exosomes mediate Zika virus transmission through SMPD3 neutral sphingomyelinase in cortical neurons. *Emerg Microbes Infect* 2019;8:307–326.
 37. Shamseddine AA, Airola MV, Hannun YA. Roles and regulation of neutral sphingomyelinase-2 in cellular and pathological processes. *Adv Biol Regul* 2015;57:24–41.
 38. Hannun YA, Obeid LM. Principles of bioactive lipid signalling: lessons from sphingolipids. *Nat Rev Mol Cell Biol* 2008;9:139–150.
 39. Lei Y, Chen L, Zhang G, et al. MicroRNAs target the Wnt/ β -catenin signaling pathway to regulate epithelial-mesenchymal transition in cancer (review). *Oncol Rep* 2020;44:1299–1313.
 40. Qiao B, He BX, Cai JH, et al. MicroRNA-27a-3p modulates the Wnt/ β -catenin signaling pathway to promote epithelial-mesenchymal transition in oral squamous carcinoma stem cells by targeting SFRP1. *Sci Rep* 2017;7:44688.
 41. Kim WK, Kwon Y, Jang M, et al. β -catenin activation down-regulates cell-cell junction-related genes and induces epithelial-to-mesenchymal transition in colorectal cancers. *Sci Rep* 2019;9:18440.
 42. Hu JL, Wang W, Lan XL, et al. CAFs secreted exosomes promote metastasis and chemotherapy resistance by enhancing cell stemness and epithelial-mesenchymal transition in colorectal cancer. *Mol Cancer* 2019;18:91.
 43. Liu P, Yang J, Pei J, et al. Regulation of MT1-MMP activity by β -catenin in MDCK non-cancer and HT1080 cancer cells. *J Cell Physiol* 2010;225:810–821.
 44. Lv X, Huang H, Feng H, et al. Circ-MMP2 (circ-0039411) induced by FOXM1 promotes the proliferation and migration of lung adenocarcinoma cells in vitro and in vivo. *Cell Death Dis* 2020;11:426.
 45. Lu K, Dong JL, Fan WJ. Twist1/2 activates MMP2 expression via binding to its promoter in colorectal cancer. *Eur Rev Med Pharmacol Sci* 2018;22:8210–8219.
 46. Lian Z, Hu Z, Xian H, et al. Exosomes derived from normal human bronchial epithelial cells down-regulate proliferation and migration of hydroquinone-transformed malignant recipient cells via up-regulating PTEN expression. *Chemosphere* 2020;244:125496.
 47. Zhu Y, Gu L, Lin X, et al. Ceramide-mediated gut dysbiosis enhances cholesterol esterification and promotes colorectal tumorigenesis in mice. *JCI Insight* 2022;7.
 48. Zheng K, Chen Z, Feng H, et al. Sphingomyelin synthase 2 promotes an aggressive breast cancer phenotype by disrupting the homeostasis of ceramide and sphingomyelin. *Cell Death Dis* 2019;10:157.
 49. Dinkins MB, Dasgupta S, Wang G, et al. Exosome reduction in vivo is associated with lower amyloid plaque load in the 5XFAD mouse model of Alzheimer's disease. *Neurobiol Aging* 2014;35:1792–1800.
 50. Jiang S, Wang Q, Feng M, et al. C2-ceramide enhances sorafenib-induced caspase-dependent apoptosis via PI3K/AKT/mTOR and Erk signaling pathways in HCC cells. *Appl Microbiol Biotechnol* 2017;101:1535–1546.

51. Debret R, Brassart-Pasco S, Lorin J, et al. Ceramide inhibition of MMP-2 expression and human cancer bronchial cell invasiveness involve decreased histone acetylation. *Biochim Biophys Acta* 2008;1783:1718–1727.
52. Zhang S, Zhou J, Zhang C, et al. Arsenic trioxide inhibits HCCLM3 cells invasion through de novo ceramide synthesis and sphingomyelinase-induced ceramide production. *Med Oncol* 2012;29:2251–2260.
53. Leonetti D, Estéphan H, Ripoché N, et al. Secretion of acid sphingomyelinase and ceramide by endothelial cells contributes to radiation-induced intestinal toxicity. *Cancer Res* 2020;80:2651–2662.
54. Chang YC, Fong Y, Tsai EM, et al. Exogenous C₆-ceramide induces apoptosis by overproduction of ROS and the switch of superoxide dismutases SOD1 to SOD2 in human lung cancer cells. *Int J Mol Sci* 2018;19.
55. Osawa Y, Suetsugu A, Matsushima-Nishiwaki R, et al. Liver acid sphingomyelinase inhibits growth of metastatic colon cancer. *J Clin Invest* 2013;123:834–843.
56. Nakagawa R, Motoki K, Ueno H, et al. Treatment of hepatic metastasis of the colon26 adenocarcinoma with an alpha-galactosylceramide, KRN7000. *Cancer Res* 1998;58:1202–1207.
57. Flowers M, Fabriás G, Delgado A, et al. C6-ceramide and targeted inhibition of acid ceramidase induce synergistic decreases in breast cancer cell growth. *Breast Cancer Res Treat* 2012;133:447–458.
58. Le Stunff H, Peterson C, Liu H, et al. Sphingosine-1-phosphate and lipid phosphohydrolases. *Biochim Biophys Acta* 2002;1582:8–17.
59. Fabriás G, Muñoz-Olaya J, Cingolani F, et al. Dihydroceramide desaturase and dihydrosphingolipids: debutant players in the sphingolipid arena. *Prog Lipid Res* 2012;51:82–94.
60. Tokuda N, Numata S, Li X, et al. β 4GalT6 is involved in the synthesis of lactosylceramide with less intensity than β 4GalT5. *Glycobiology* 2013;23:1175–1183.
61. Yoo TH, Pedigo CE, Guzman J, et al. Sphingomyelinase-like phosphodiesterase 3b expression levels determine podocyte injury phenotypes in glomerular disease. *J Am Soc Nephrol* 2015;26:133–147.
62. Muñoz-Guardiola P, Casas J, Megías-Roda E, et al. The anti-cancer drug ABTL0812 induces ER stress-mediated cytotoxic autophagy by increasing dihydroceramide levels in cancer cells. *Autophagy* 2021;17:1349–1366.
63. Furukawa K. Challenge to the suppression of tumor growth by the β 4-galactosyltransferase genes. *Proc Jpn Acad Ser B Phys Biol Sci* 2015;91:1–16.
64. Heinz LX, Baumann CL, Köberlin MS, et al. The lipid-modifying enzyme SMPDL3B negatively regulates innate immunity. *Cell Rep* 2015;11:1919–1928.
65. Zhong L, Kong JN, Dinkins MB, et al. Increased liver tumor formation in neutral sphingomyelinase-2-deficient mice. *J Lipid Res* 2018;59:795–804.
66. Montfort A, Bertrand F, Rochotte J, et al. Neutral sphingomyelinase 2 heightens anti-melanoma immune responses and anti-PD-1 therapy efficacy. *Cancer Immunol Res* 2021;9:568–582.
67. Mathivanan S, Ji H, Simpson RJ. Exosomes: extracellular organelles important in intercellular communication. *J Proteomics* 2010;73:1907–1920.
68. Valadi H, Ekström K, Bossios A, et al. Exosome-mediated transfer of mRNAs and microRNAs is a novel mechanism of genetic exchange between cells. *Nat Cell Biol* 2007;9:654–659.
69. Li S, Wu Y, Ding F, et al. Engineering macrophage-derived exosomes for targeted chemotherapy of triple-negative breast cancer. *Nanoscale* 2020;12:10854–10862.
70. Kim MS, Haney MJ, Zhao Y, et al. Development of exosome-encapsulated paclitaxel to overcome MDR in cancer cells. *Nanomedicine* 2016;12:655–664.
71. Morad SA, Cabot MC. Ceramide-orchestrated signalling in cancer cells. *Nat Rev Cancer* 2013;13:51–65.
72. Morad SA, Bridges LC, Almeida LA, et al. Short-chain ceramides depress integrin cell surface expression and function in colorectal cancer cells. *Cancer Lett* 2016;376:199–204.
73. Morad SA, Madigan JP, Levin JC, et al. Tamoxifen magnifies therapeutic impact of ceramide in human colorectal cancer cells independent of p53. *Biochem Pharmacol* 2013;85:1057–1065.
74. Mitchell C, Willenbring H. A reproducible and well-tolerated method for 2/3 partial hepatectomy in mice. *Nat Protoc* 2008;3:1167–1170.
75. Yu J, Green MD, Li S, et al. Liver metastasis restrains immunotherapy efficacy via macrophage-mediated T cell elimination. *Nat Med* 2021;27:152–164.
76. Sands MS. AAV-mediated liver-directed gene therapy. *Methods Mol Biol* 2011;807:141–157.
77. Matyash V, Liebisch G, Kurzchalia TV, et al. Lipid extraction by methyl-tert-butyl ether for high-throughput lipidomics. *J Lipid Res* 2008;49:1137–1146.

Received December 24, 2022. Accepted May 22, 2023.

Correspondence

Address correspondence to: Jie Zhou, MD, Division of Hepatobiliopancreatic Surgery, Department of General Surgery, Nanfang Hospital, Southern Medical University, 1838 North Guangzhou Avenue, Guangzhou 510515, Guangdong, China. e-mail: jacky@smu.edu.cn; or Jun Yan, PhD, Department of General Surgery, Guangdong Provincial Key Laboratory of Precision Medicine for Gastrointestinal Tumor, Nanfang Hospital, The First School of Clinical Medicine, Southern Medical University, 1838 North Guangzhou Avenue, Guangzhou 510515, Guangdong, China. e-mail: yanjunfudan@163.com; or Chuanjiang Li, PhD, Division of Hepatobiliopancreatic Surgery, Department of General Surgery, Nanfang Hospital, Southern Medical University, 1838 North Guangzhou Avenue, Guangzhou 510515, Guangdong, China. e-mail: licj@smu.edu.cn.

Acknowledgments

The authors acknowledge the technical support provided by the Central Laboratory of Southern Medical University, Guangzhou, Guangdong, China for lipidomic analyses.

CRedit Authorship Contributions

Qingping Li (Conceptualization: Lead; Data curation: Lead; Formal analysis: Lead; Writing – original draft: Lead)

Kai Wang (Conceptualization: Lead; Funding acquisition: Supporting; Supervision: Lead; Writing – review & editing: Lead)

Jieyuan Li (Conceptualization: Lead; Data curation: Lead; Formal analysis: Lead)

Leyi Liao (Methodology: Supporting; Validation: Supporting)

Yiyi Li (Methodology: Supporting; Formal analysis: Supporting)

Hanbiao Liang (Methodology: Supporting; Validation: Supporting)

Can Huang (Methodology: Supporting; Validation: Supporting)

Jian Gan (Methodology: Supporting; Validation: Supporting)
Xiaoyu Dong (Methodology: Supporting)
Yaowen Hu (Methodology: Supporting)
Jiaxin Cheng (Methodology: Supporting)
Hongli Ji (Methodology: Supporting)
Cuiting Liu (Methodology: Supporting)
Minghui Zeng (Methodology: Supporting)
Sheng Yu (Methodology: Supporting)
Biao Wang (Methodology: Supporting)
Jianping Qian (Methodology: Supporting)
Zhongshun Tang (Methodology: Supporting)
Yonghong Peng (Methodology: Supporting)
Shanhua Tang (Methodology: Supporting)
Mengxuan Li (Methodology: Supporting)
Jie Zhou (Conceptualization: Supporting; Funding acquisition: Supporting;
Data curation: Lead; Supervision: Supporting)

Jun Yan (Funding acquisition: Supporting; Project administration: Lead;
Writing – review & editing: Lead)

Chuanjiang Li (Conceptualization: Lead; Data curation: Supporting; Formal
analysis: Supporting; Funding acquisition: Lead; Supervision: Lead; Writing –
review & editing: Lead)

Conflicts of interest

The authors disclose no conflicts.

Funding

Supported by the National Natural Science Foundation of China (82070642, 82170647, 82273360, and 82270661), the Guangdong Basic and Applied Basic Research Foundation (2021A1515012485, 2020A1515011205, and 2021A1515012146), the Guangdong Provincial Key Laboratory of Precision Medicine for Gastrointestinal Cancer (2020B121201004), and the Science and Technology Planning Project of Guangzhou City (202206010085).